

# Design and Simulation of 5-Bit DMTL Phase Shifter with Improved RF Switch Incorporation of Stress Regions

<sup>1</sup> G Srihari, <sup>2</sup> T. Shanmuganantham

<sup>1,2</sup> Department of Electronics Engineering, Pondicherry University, Puducherry, India 605014  
srihari.nan@gmail.com, shanmugananthamster@gmail.com

Received: 01st July 2020, Accepted: 27th July 2020, Published: 31st August 2020

## Abstract

The MEMS technology was the most adopted technology in recent years in the field of Communication which involves the RF devices. Rapid changes have been incorporated in passive component design with use Microsystems, having immense advantage over traditional with small size, better performance and compatibility with limited energy usage. Among, Phase shifters which have seen evidence development after the RF MEMS switch are brought forward as extension of RF switches itself. With broadband operating frequency ranges, evolving by minimizing the limitations of basic phase shifters possess. As DMTL phase shifter taken its prominence among other types, where the capacitive switch has major role in determining the performance in terms of speed. As techniques like pull-in voltage base techniques are least efficient in achieving the higher speeds, the mechanical tuning of the devices without altering the dimensions are preferred. In this paper a DMTL phase shifter that actuates with capacitive method is having modified beam structure to improve the frequency of the beam thus by enhancing the switching speed is adopted. With incorporation of the slits on the beam, switching speed is enhanced by 6-7%, that operates at wide band applications from 18-40 GHz.

## Keywords

MEMS; DMTL; Phase Shifters; RF MEMS Switch; Switching Time.

## Introduction

The concept of Micro-machining technology that incorporates the science of Micro-electromechanical Systems (MEMS) and devices associated developed by Harvey C. Nathanson in 1965. This technology has gained its importance in all the fields of engineering and applications. Having the more advantageous with the traditional devices and systems, they possess the attributes of small in size, higher performance and better sensitivity and resolution making the MEMS more familiar in mechanical to biomedical industries. It gained the importance with Sensors and Actuators brought forward using this MEMS technology and various accelerometers are reported in literature [1-4]. This technology was brought to the applications of Radio frequency, since having the advantages of high performance in scaled down application, and in high frequency ranges. As in course with the upcoming of Millimeter wave base, the need for integration and scaling down the systems are essentials, the incorporation of MEMS technology is evident. This has given to the division of RF MEMS devices, being replacement for the traditional semiconductor based devices. In foremost RF MEMS switches are one, where extensive research and design modification have done so far since incorporation of Micro-machining was started in this field. As a result conventional PIN, MOSFET and GaAs based devices are replaced with RF MEMS switches.

Though the RF MEMS devices have advantages being the replacements, still have substantial challenges and setbacks when considering to operate at higher frequencies. RF passive devices like Phase shifters, couplers, splitters etc are quite more complicated with consideration of losses in terms of mechanical aspects rather than signal base loss mediums. As the MEMS deals with design that might consists of mechanical components, devices are prone to more loss concerned with vibrational and material base. One such device that has been in literature was RF MEMS base Phase Shifter which has wide application in RADAR and Wireless applications [5]. These devices are the considered to be two port devices, that are intended for the phase change from one port to another with loss less transmission of the signal. The conventional devices are designed with the help of PIN diodes, faced the challenges of low switching speed and design consideration. When these are replaced with the Field effect transistors, overcome the switching speed constraint but suffered with the transmission loss which is reported to be around 4-6 dB, and it is even higher with 8-9 dB for 12-18 GHz and 35 GHz [6-10]. Few reported works have done the phase shifter with Barium titanate, that works with the Ferro-electric [11] are having the advantage of tuning but losses and cost are compromised.

In recent times, the RF passive components are adopted with the Micro-machining and calling down approaches with incorporation of the MEMS technology and the most adopted device with incorporation of MEMS technology was phase shifter. As the phase shifter using the MEMS technology is evolved with the RF MEMS switch design as the

basic element. These RF MEMS switches are designed for various frequencies and with improved performance, by reducing the losses. This improvements brought the solution to challenges that traditional device are facing and cost of the devices are also brought down [11-13]. With this the Phase shifter as evolved with analog and digital base. Where Distributed Line (DTL), Loaded -line, reflection type and switched line are considered to be the categorized configurations of the shifter as per the design considerations. Among them DTL is also referred as the DMTL, most of the literature reported DMTL are analog within early 2000, with the introduction of digital communication and rapid development the urge for the digital base DMTL are very much needed. The main advantage with these, they are fabricated with most evident material silicon, ensuring the minimal cost and Losses at high frequency of operations [14]. But the challenges with this DMTL is having performance issues as the MEMS switches - basic building blocks of Shifter device having mechanical actuating element. This actuating element tend show instability at higher frequency of operations. There is always a compromise in speed and performance due this actuation element, as the larger the size more mechanical stability but less in frequency of actuation and vice versa. Another challenge lies with the fabrication of the devices at micro scale, which involves process other than silicon as well, even makes the things more worse.

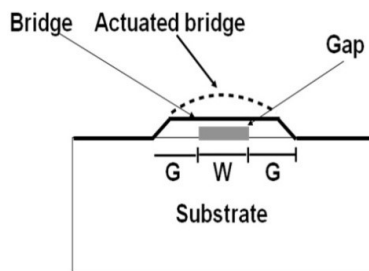


**Fig. 1: RF MEMS Switch with Capacitive Actuation.**

The present work is to emphasise on the mechanical stability improvement of the DMTL phase shifter which operates at the wide band from 18GHz to 40 GHz, using Metal- Insulator- Metal configuration. The performance and the stability are improved by the incorporation of Stress concentrated region on the beam of the RF MEMS switch which is basic element of the shifter. For improving faster switching, pull-in voltage, beam dimensional scaling and material alteration are mostly preferred in the literature, where the there is limitation of other parameters. But improving the device stability by stress concentration regions does alter the majority of devices considerations, but emphasis on the improvement of the frequency of the beam and thus switching speed is enhanced.

#### DMTL Phase Shifter

The design of the DMTL shifter is consider with the RF MEMS switch either in the configuration of Metal-Air-Metal (MAM) or Metal-Insulator-Metal (MIM) base configuration on a coplanar waveguide (CPW). Generally the material preferred for the CPW to place on a substrate is glass. Upon this CPW, a bridge configuration was constructed, which acts as simple RF MEMS switch that acts as the capacitive, since the bridge and the CPW plane acts as conductive plates. These two plates can be referred as the DC plate and RF connector plate and a gap between the two plates which acts the air gap for MEMS based capacitive switch. In between a dielectric was placed generally any oxide layer that acts as the insulator [14]. When an DC voltage is applied to the MEMS switch with a unified line, posing high resistance, the bridge breaks upon the application of the voltage and inline transmission of the wave is shifted. Generally any transmission line is expressed in terms of capacitance, inductance and resistance  $L_t$ ,  $C_t$  and  $R_t$ . This can represented with an electric circuit model in Fig 2.

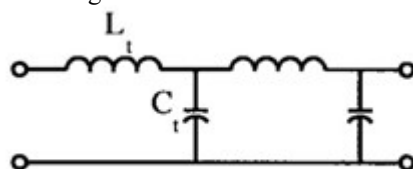


**Fig. 2: Transmission Line in terms of Capacitance, Inductance and Resistance.**

This entire configuration makes as RF MEMS switch configuration, so as for a phase shifter RF MEMS switch is basic block of it. When DC voltage applied to the Switch, the bridge is in down state that is actuated and when it was made to high resistance, simultaneously bridge becomes un actuated and opens up. In un actuated state only the AC capacitance is present and actuated state the charge built was discharged. In order to bias this switch also referred as

pull-in voltage, a single high resistance line is used, this line was initially connected to one of the device and later moving it from switch to switch by bias line. This bias line has some in built resistance  $R_b$ . In most of the DMTL phase shifters, tuning of performance characteristics of the device are done using this  $R_b$  and placing an inductor in series to this resistance by connecting to the RF connector plate where the bridge makes contact with it. This provides the discharge of the charge in more efficient way and any residual. This makes the bridge to be activated for charge in next cycle very much effectively. This tuning is expected to make the switching off the circuit faster by electric tuning of the device. But this technique has saturation with certain challenges, meeting the requirements with fabrication in certain time has limitation and other as bulking of the more inductance and capacitance might require higher pull in voltage making the design difficult for low power applications. Fig.3 explains the electric equivalent circuits of the single DMTL phase shifter under up state and down state. Further in this paper, the approach of mechanical tuning of the DMTL was made by applying the concept of the stress concentration regions. As the MEMS based RF switches are superior than the solid state devices, less pull-voltage, capable of handling high power and having lower spring constant are major challenges [15-17]. With adaptation of spring constant ( $K$ ) for the mechanical beam, which increases the actuate area of the switch electrodes and fine tuning the gap between the actuation electrodes, are concerning parameters to reduce the pull-in voltage. The stress controlled regions on the actuating beam will certainly help in reducing the up-state capacitance, that is major cause for insertion loss and in parallel with down state capacitance is modelled with high relative permittivity and thin film dielectric property for further increase to enhance the isolation property.

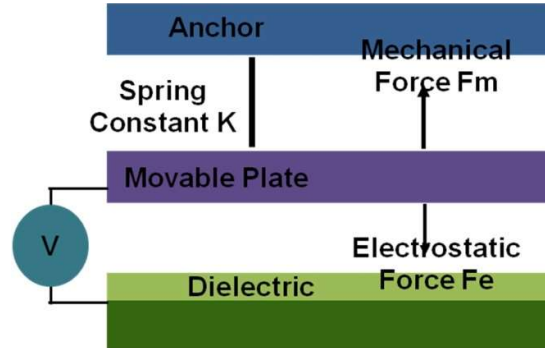


**Fig. 3: Single DMTL Phase Shifter Under Up State and Down State.**

## Proposed Wide-Band DMTL

### A. Design and Structure of RF Switch

It was mentioned in the section I, that phase shifters with MEMS technology are designed with the RF MEMS switch as the basic element. These was one way or other are alternative replacements for the solid state base devices. For this, it is concluded that the switch design was very important and prominent in modeling the Phase shifter at micro scales, involving the mechanical actuating elements. Challenges of the RF MEMS switch in terms of mechanical and the correlation of the mechanical aspects that alter the electric and capacitance parameters are discussed in Section II, are endorsed in this paper, as most of the RF MEMS switch design, the actuating element is considered to cantilever or beam. As both of them are subjected to the spring constant, up state capacitance are the more prone for alterations. All this, along with the fabrication challenges will question the performance and stability of the devices which are intended for use in wide application themes. As both of them are subjected to the spring constant, up state capacitance are the more prone for alterations. All this, along with the fabrication challenges will question the performance and stability of the devices which are intended for use in wide application themes. This is because, when the beam length is varied, that alters the CPW dimensions which changes the operating frequency and might increase the loss. The phase shift achieved, with these kind of alternation have the direct dependency on the operational wavelength ( $1/\lambda$ ) and effective length ( $L$ ). As the DMTL is constructed by the serial loading of the transmission line (TL). This was further loaded with MEMS based massive components like inductors and capacitors. As these was in another way explained to be the RF capacitive Switch which has the actuating element as discussed earlier shown in Fig 2. The mechanical element that was proposed in this work is beam base. In such design the actuating element will be the top plate of the capacitor and the waveguide at the bottom being the ground plane.

It was observed the slow behaviour of the transmitted wave ( $V_p \ll c$ ), where  $V_p$  = phase velocity and  $C$  is velocity of light in vacuum. These are crucial parameters for the design of DMTL based phase shifter [18]. The capacitance is calibrated in these kinds of system with dynamic actuation of the actuating plate, which is done in plane deflection. This can be inferred as the parallel plate capacitor, but where one plate is having the dynamic nature. As these bridges are actuated by the external forces, and in case of the RF MEMS base passive components involving switches are

actuated by the pull-in voltage. This is the subject that explains the upstate and down state of the device. Such device when constructed in series with unified CPW, makes things more complex and complicated in terms of performance etc. In such conditions the pull-in voltage in more complex parameters which needs to modeled. This work is approached with the wideband switch that is operated at 8-40 GHz [3,19], that are reported in 1999, and further improved to make DMTL. As improvement of MEMS based micro-structures like single pole-double throw mechanics switches, that made to bring forward the digital base shifters. In most of the designs the microwave passive devices are preferred with the silicon and glass are major substrate materials and in case of the switch, thin film was deposited with silicon oxide, since the feasibility of fabrication processes. As switch consisting of the mechanical element, is subjected to stress and strain upon actuation and as switch is subjected numerous operations, stress and strain will tilt up with the hysteresis losses that won't be coming back to normal leaving behind, molecular disarrangement that creates the structural failure. So, the stress and strain with the different load conditions to be observed and time base analysis is must to understand the long terms functionality of the device and the Young's modulus was the deciding factor for this. Another challenging factor is switching speed. The switching speed depends upon the charge and discharge patterns of the capacitance that was built. But in case of MEMS switch, the frequency of the beam is responsible which is resonant frequency of the beam. It has the dependency on the pull-in voltage as well. As the residual charge that was left over also adds on to the next charge-discharge cycle.

The major functionality is considered with performance of the capacitive switch, which is intends upon the switching time( $t_s$ )- the time required from on/off. The switching time depends on the eq. 1 which is shown below

$$T_s = \frac{3.67 * V_p}{V_s \omega} \quad (1)$$

Where  $V_s$  is source voltage and which is incremented by 1.4 times of the actuation voltage in DMTL variety of base phase shifter using capacitive type switching. By altering this condition the above equation is further simplified to

$$T_s = \frac{2.62}{\omega} \quad (2)$$

Modifying the above equation the with the spring constant of the mechanical actuator

$$T_s = 2.67 \sqrt{m/k} \quad (3)$$

This endorsed the implication regarding the frequency of switching action will depend on with respect to the length, width and thickness of the actuating element. In this paper, we have concentrated on the stress-controlled regions to un-alter the actuator lengths but to improve the frequency of switch that minimize the switching speed and further relates to fast switching[22].

### B. Functionality

As it was discussed in above, the functionality of the phase shifter depends upon the switch operations. In this proposed device, switch is electrostatically actuated by using the capacitive MEMS switch, that is configured in shunt bias configuration. The actuating beam is placed on the top of CPW line. The capacitive switch is fixed on both sides of the of the CPW by separating it from the signal transmission line. In initial condition switch is up state and with the application of the voltage, it moves towards the dielectric state with deflection and this is referred as the down state. The switch is made simultaneously ON and OFF state with the this application of external voltage which are shown in the Fig 4.

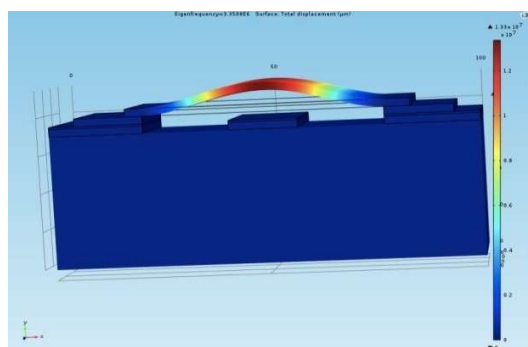


**Fig. 4: RF MEMS Switch with Upstate.**

### C. Material Selection

Material selection was crucial in terms of fabrication, design and performance of the device, in this paper the material selection was done with parametric analysis was done for understanding the material properties and their behaviour with respect to the design. The final material selection was done with the principle of Ashby's material selection process, that examples three basic guidelines for material selection for the device. According to Ashby's principle concept, embodiment and detail are major steps that governs the material selection. So as per this, the switch design depends upon the materials of the bring that defines the mechanical properties like spring constant, elasticity etc and dielectric material property that to built the charge. When these are chosen abruptly, chances of effecting the pull in voltage, switching speed and reliability of the devices are altered.

In order to choose the material for the beam and dielectric, a parametric sweep is carried out using Finite element Modeling (FEM) tool with different materials in consideration. An analysis between the Young's Modulus and thermal conductivity of different materials would certainly help in choosing the beam material for selection, in order to minimize the low pull in voltage. So that high conductive materials are compared in this analysis (Au, Pt, Ni, Cr, Nb, Al<sub>2</sub>O<sub>3</sub>) etc. as shows in Fig 6. And properties like insertion and isolation off RF passive components. It was mentioned in literature that, higher the Poisson ratio, the better capacitance is built between the dielectric and the beam. So, material having the higher Poisson's ratio are shown in the Table 1.

For the above table the, Silicon Nitride having the higher poisson's ratio, in most of the devices silicon oxide layer is preferred for its convenience of fabrication. But with techniques like Chemical Vapor Deposition techniques growing of silicon Nitride is also less complicated.

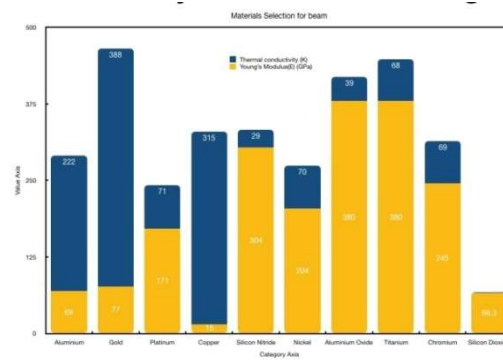


**Fig. 5: Young's Modulus and Thermal Conductivity of Different Materials**

**Table 1: Material Properties for Beam Consideration.**

Materials	Properties	
	Young's Modulus(GPa)	Thermal Conductivity(K)
Aluminium	1521.91	1518.75
Gold	2185.32	2183.67
Platinum	3043.82	3042.12
Copper	15	315
Silicon Nitride	304	29
Nickel	204	70
Aluminium Oxide	380	39
Titanium	380	68
Chromium	245	69
Silicon Dioxide	66.3	1.3

### D. Stress Regions/Perforations

In the proposed device of the DMTL, that uses the switch is incorporated with the perforation in order to improve the performance in terms of its switching speed which are shown in Fig 7. The perforation would help the device is minimizing the mass of the beam, which makes the frequency to be in higher state than usual calibrated resonant

frequency. This will render the need of improving the switching speed and reduces the pull in voltage. But the challenges lies in making the perforation on the beam, that might alter the stability and reliability of the beam for longer durations. So a minimal perforation and maximum frequency shift is method that can be adopted to retain the stability and ensure frequency is in higher note. So regularization of the holes and balancing on the beam either side is important in tuning the frequency of the beam and it was stated that balanced perforation on top of the device would certainly improve the device frequency[23].

The main idea of this method is enhance the stress that to develop in the cantilever or beam and this technique does not involve any complex process of the micro-fabrication. With simple techniques by masking and etching, the perforation are framed. Initially this was reported for piezoresistive based MEMS sensor where sensitivity can be enhanced with larger amounts of stress [21]. In this paper, this approach was adopted to decrease the effective mass of the cantilever without altering the dimensions and shape of the beam. As from eq. 3 it can be stated that mass of the cantilever is inversely proportional to the frequency of the beam, where mass decreases the frequency increases. But too many perforation might increase the stress developed in the device that might alter the number switching of the device as it is involved with mechanical structures in it. In this design, as approach of the beam is utilized where the perforations are to balanced for beam being fixed at the both rear ends.

The perforations are made so in balanced state, either side of the beam to its centre and observed that frequency much better improved when the perforation are close to centre. As it was ensured that the set perforation are separated by equidistant, so that maximum deflection happens at the centre of the beam. The distance was measured to 4 micron and the each slit has 2 micron of each side (Square Shaped) and having 500 nm thickness as shown in Fig. 9. In such MEMS structure, we have observed principle mode frequency to be around 949 KHz.

#### **Pull-In-Voltage**

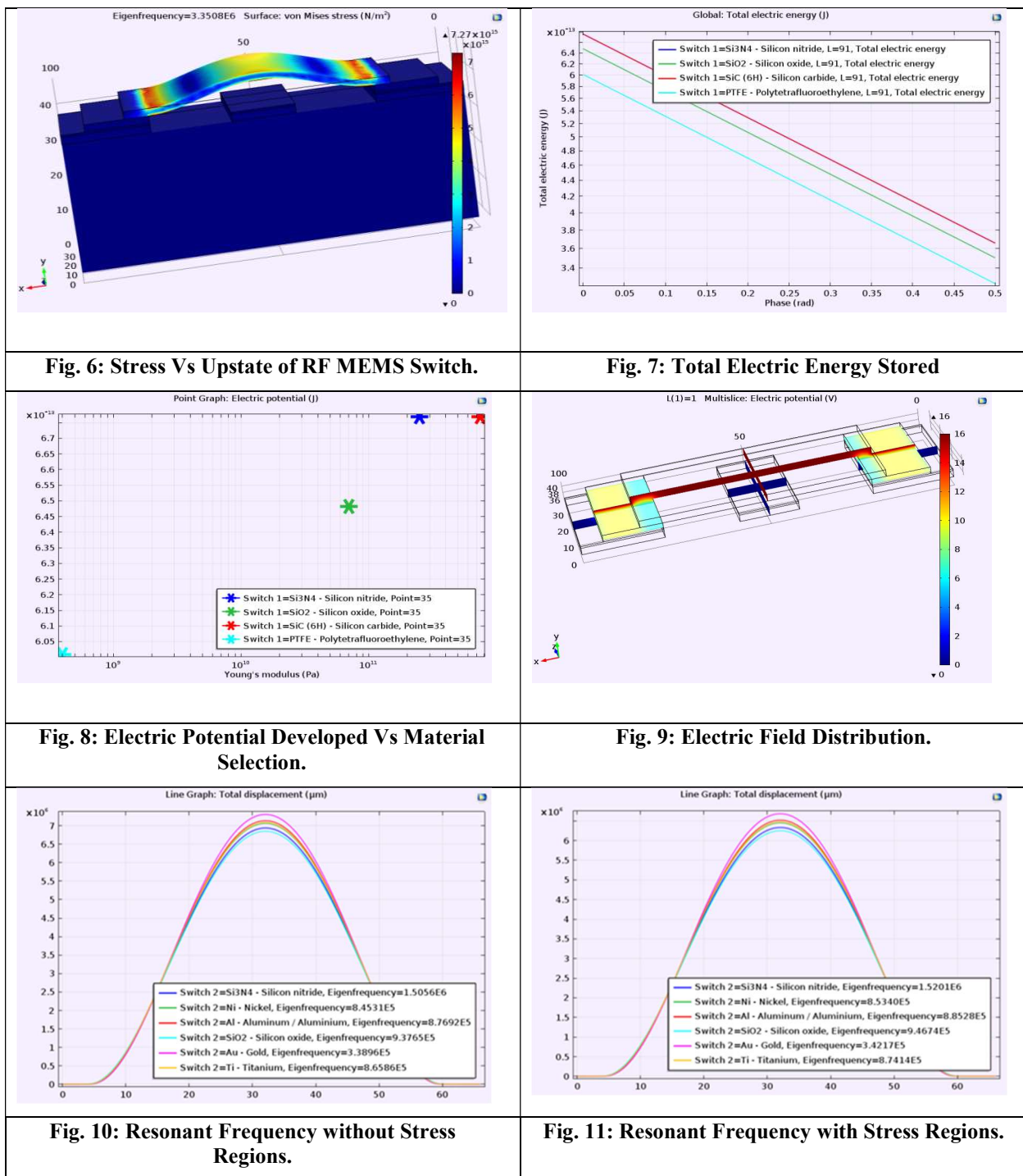
The approach of capacitive RF MEMS switch, one plate is fixed and the other plate is movable, with electrostatic actuation by the force created upon the application of the voltage between the top and bottom plates. With the help of restoration force ( $F_m$ ) and restoration force ( $F_e$ ), the motion of the plate is influenced.

$$V_p = \sqrt{8K / 27\epsilon A g^3} \quad (4)$$

where K is spring constant,  $\epsilon$  is permittivity, A is area in millimeters and g is young's modulus.

#### **Simulation of the DMTL**

The RF capacitive MEMS switch, is designed with the above mentioned parameters and materials using the Finite Element Modeling (FEM) tools like COMSOL Multiphysics. In this mechanical behaviour and the resonant frequency of the switch are assessed and compared with and without SCR. Material sweep was performed to analyze the beam resonant frequency with variation to Young's Modulus of the device. The charge built during the up state was calibrated using the electrostatic AC/DC analysis in the tool by fixing the constraints and two parallel plates. For structural analysis the boundary conditions are ensured taken care of like fixing the beam on the rear ends for operating the beam in principle mode. The charge accumulated for an initial switch is around 70 pF and each switch provides a shift of 6 degrees which regarded as the phase difference. With the shunt configuration of these capacitive switch bridges the designed phase shift can be achieved. In terms of Radio frequencies these kind of device acquire insertion loss and gain are the parameters that needs to considered. But along with that speed of the switch is other parameter that was discussed earlier. As the speed of the device is tuned with the pull-in voltage, but as the device consists of the mechanical structure, tuning mechanical would be more advantageous which might improve the overall performance of the device. So, with incorporation of the slit base devices, the main advantage is that beam frequency can be increased that alters the switching speed and this can be achieved without altering the dimensions of the devices. When the Eigen frequency analysis was carried for a single switch, has showed the frequency improvement by 59 KHz from 890 KHz to 949 KHz thus modified switch showing 6 to 7 % improvement which is considerable to make modified DMTL operate much faster than the traditional DMTL. The main challenges that has to be considered in this design was to ensure that minimum strain was developed due to the slits on the beam, which might deform the device has to compromise overall durability of the device.



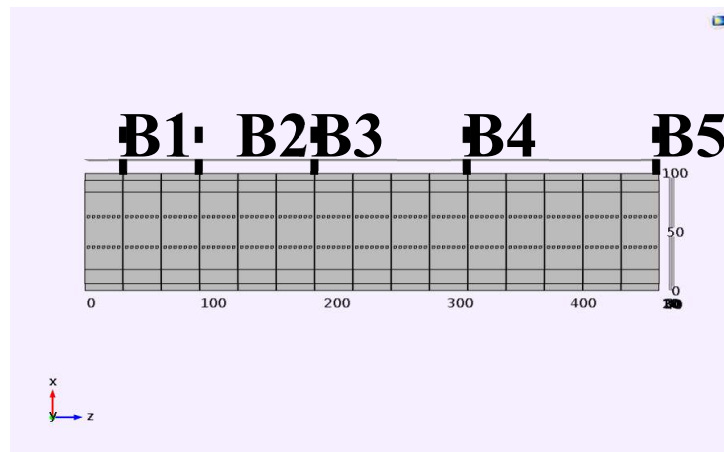


Fig. 12: 5-Bit DMTL Phase Shifter.

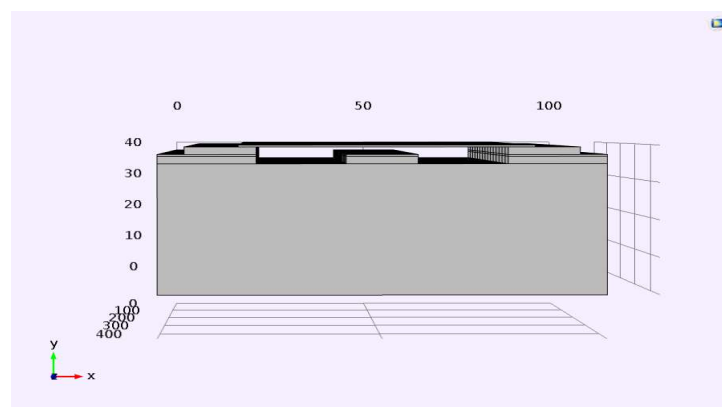


Fig. 13: Side View of Phase Shifter.

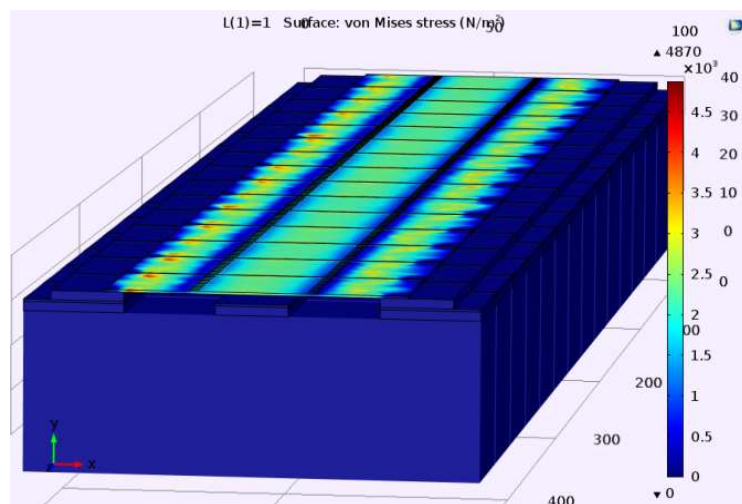
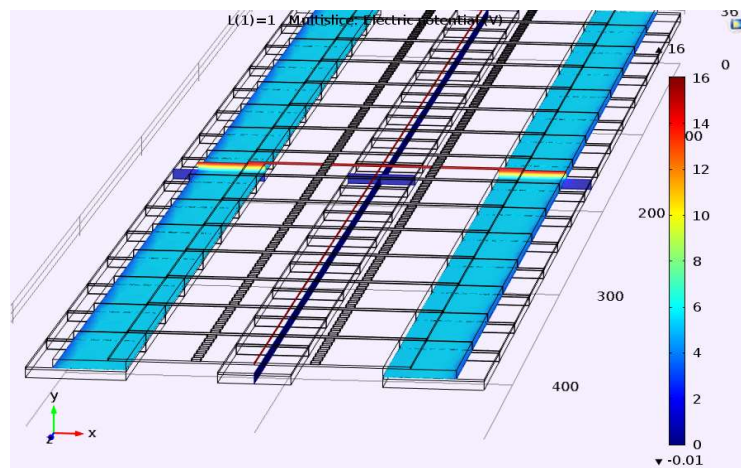
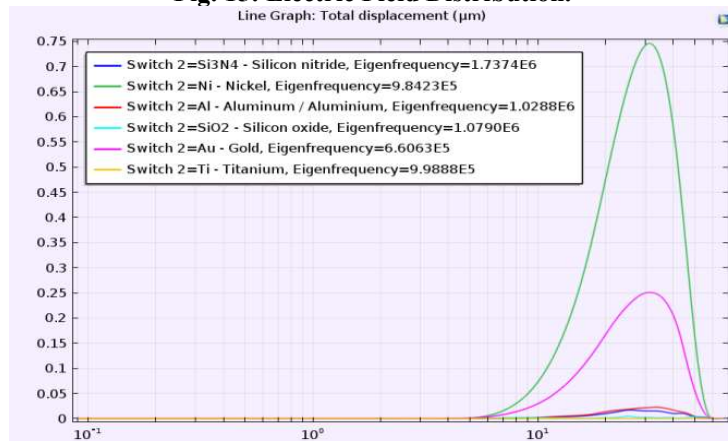


Fig. 14: Stress Developed Phase Shifter during Excitation.

**Fig. 15: Electric Field Distribution.****Fig. 16: Frequency Analysis of the Device.**

### Conclusion

The 5 bit DMTL phase shifter using modified switch that has built with stress concentration regions, it showed increase in the speed by resonant frequency changes of the beam and in parallel the pull voltage was also reduced. They was 8 % increase in switching speed of the device and pull in voltage was constraint to 12 V. This paper has limited to the study of single bit calculation of the speed and has meet the overall speed and comparison with fabrication needs validated as future study.

### Acknowledgements

This work is supported by the Pondicherry University, Puducherry to develop my academic and research knowledge by permitting me to do research work in the field of MEMS Phase shifters.

### References

1. M. Makimoto and S. Yamashita, "Compact band-pass filters using stepped impedance resonators", *IEEE Trans. Microwave Theory Tech.*, Vol. 40, pp. 16-19, Jan. 1979.
2. G.L. Mathieu, L. Young and E.M.T. Jones, *Microwave Filters, Impedance-Matching Networks and Coupling Structures*, 1<sup>st</sup> ed., Artech House, Massachusetts, 1980.
3. S. Singh, "Design of microwave wideband impedance matching networks", M.S thesis, Dept. of Electrical Engineering, University of Nevada, Reno, USA, December 1995.
4. S.L. March, "Empirical formulas for the impedance and effective dielectric constant of covered microstrip for use in MIC CAD", *Proc. European Microwave Conf.*, Microwave Exhibitors & Publishers Ltd., Kent, U.K., pp. 671-676, Sept. 1981.
5. H. Ogawa, "Technologies and standardization of milli meter-wave wireless personal area network", *Digest of 10<sup>th</sup> International Symposium on Microwave and Optical Technology*, Fukuoka, Japan, pp. 12-14, August 22-25, 2005

6. O. Access, "We are Intec Open , the world ' s leading publisher of Open Access books Built by scientists , for scientists TOP 1 % Based Sensor by Introducing Stress."
7. A. F. Recon, R. F. Mem, and P. Shifter, "A 15–40-GHz Frequency Reconfigurable RF MEMS Phase Shifter," vol. 61, no. 8, pp. 2865–2877, 2013.
8. Nguyen, C.T.-C.; Katehi, L.P.B.; Rebeiz, G.M. Micromachined Devices for wireless communications. Proc. IEEE 1998, 86, 1756-1768.
9. Yao, J.J. RF MEMS from a device perspective. J. Micromech. Microeng. 2000, 10, R9–R38.
10. K. Van Caekenbergh and T. Vähä-heikkilä, "An Analog RF MEMS Slotline True-Time-Delay Phase Shifter," pp. 1–9, 2008.
11. V. Nassereddine, "Milli meter-wave phase shifters based on tunable transmission lines in MEMS technology post-CMOS process To cite this version : HAL Id : tel-01492907 Déphasateurs en bande millimétrique basés sur des lignes à ondes lentes accordables en technologie MEMS dans un process post-CMOS .," 2018.
12. G. Mcfeeters and M. Okoniewski, "With Enhanced Tuning," vol. 16, no. 1, pp. 34–36, 2006.
13. B. Lakshminarayanan, T. M. Weller, S. Member, and A. Abstract, "Design and Modeling of 4-bit Slow-Wave MEMS Phase Shifters," vol. 54, no. 1, pp. 120–127, 2006.
14. B. Lacroix, A. Pothier, A. Crunteanu, and P. Blondy, "Phase Shifter Design Based on Fast RF MEMS Switched Capacitors," no. October, pp. 478–481, 2008.
15. S. Afrang and Æ. B. Yeop, "Distributed transmission line phase shifter using MEMS switches and inductors," pp. 1173–1183, 2008.
16. T. De Lauretis, A. Huyssen, and K. M. Woodward, "The Technological imagination : theories and fictions," Theor. Contemp. Cult. ; 3, no. 1, p. 201, 1980.
17. U. M. Spt, S. Switches, S. Dey, S. Member, and S. K. Koul, "Reliability Analysis of Ku-Band 5-bit Phase Shifters," vol. 63, no. 12, pp. 3997–4012, 2015.
18. C. R. Dietlein, S. Member, S. S. Bedair, J. S. Pulskamp, C. D. Meyer, and R. G. Polcawich, "Micro fabricated Thick-Cu PZT-MEMS Millimeter-Wave Topologies and Devices," vol. 25, no. 3, pp. 163–165, 2015.
19. S. Gong, S. Member, H. Shen, and N. S. Barker, "A 60-GHz 2-bit Switched-Line Phase Shifter Using SP4T RF-MEMS Switches," vol. 59, no. 4, pp. 894–900, 2011.
20. N. Kingsley, S. Member, J. Papapolymerou, and S. Member, "Organic ' Wafer-Scale ' Packaged Miniature," vol. 54, no. 3, pp. 1229–1236, 2006.
21. S. K. Koul and S. Dey, "K -Band 4-Bit Phase Shifter Using Two Back to Back MEMS SP16T Switching Networks," pp. 1–13, 2018.
22. K. S. Rao, C. H. G. Chand, and K. G. Sravani, "Design , Modeling and Analysis of Perforated RF MEMS Capacitive Shunt Switch," IEEE Access, vol. 7, pp. 74869–74878, 2019.
23. E. Rufus and A. C. Actuation, "MEMS Capacitive Switch with Stress Concentration Regions for Wide band Applications Speed Applications," 2019 Int. Conf. Vis. Towar. Emerg. Trends Commun. Netw., pp. 1–5, 2019.

# Broadband substrate-integrated waveguide venus-shaped slot antenna for V-band applications

Nanda Kumar Mungaru  |

Shanmugannatham Thangavelu 

Department of Electronics Engineering, School of Engineering and Technology, Pondicherry University, Pondicherry, India

## Correspondence

Shanmuganantham Thagavelu, Department of Electronics Engineering; School of Engineering and Technology, Pondicherry University, Pondicherry 605014, India.

Email: shanmugananthamster@gmail.com

## Abstract

In this article, broadband substrate-integrated waveguide (SIW) venus-shaped slot antenna for V-band applications was proposed. The size of the antenna is  $13 \times 9 \times 0.381$  mm and printed in a 5880 RT-Duriod substrate with a dielectric constant of 2.2. The antenna is designed, simulated, tested, and validated in terms of reflection coefficient and voltage standing wave ratio. The impedance bandwidths of the simulated and measured results are 5.4 GHz (ranging from 57 GHz to 62.4 GHz) and 5.3 GHz (ranging from 57.15 GHz to 62.45 GHz) and also good bidirectional radiation patterns are obtained. Finally, the Resistor, Inductor, Capacitorleave (RLC) equivalent circuit model is introduced to match the reflection coefficient of an antenna, implemented with the help of MATLAB and validated.

## KEYWORDS

matrix laboratory, millimeter waves, substrate-integrated waveguide, venus-shaped slot

is a type of unlicensed frequency in the millimeter wave band and mostly preferred for narrow beam, high data rate, and short-range applications and for less interference. The frequency band ranges from 57 GHz to 64 GHz; and as per the Federal Communication Commission standards it is 7 GHz, but a minimum of 3 GHz is sufficient to fulfill this application. This is used for millimeter wireless applications like wireless LAN (WLAN), automotive applications, gigabit wireless fidelity (Gi-Fi), and 5G communication applications. Some of the literature studies were discussed as follows: Bakhtafrooz and Borji<sup>1</sup> are the first scientists who introduced antenna for millimeter wireless applications and shapes consisting of stack of layers, which were of  $4 \times 4$  and  $6 \times 6$  arrays, respectively. Tomas et al.<sup>3</sup> introduced array-based microstrip patch antenna fed by microstrip for high gain applications with  $6 \times 8$  array and the impedance bandwidth of 1.1 GHz and gain is 21.6 dBi. The “substrate-integrated waveguide (SIW)” feed SIW-based slot antenna was proposed by Gong and his team<sup>4</sup> for millimeter wireless applications and investigated a wide width slot to satisfy the operating band of millimeter wireless applications, where the impedance band width is 3.25 GHz and gain is 6 dBi.

Srivastava et al<sup>5</sup> proposed an SIW feed “antipodal linear tapered slot antenna (ALTSAs)” for millimeter wireless applications, and it has a resonant frequency of 60 GHz with 1.5 GHz bandwidth, gain of 16.3 dBi, and slot loaded with different dielectric shapes for gain improvement that are rectangular, triangular, and exponential. Ramesh et al<sup>6</sup> introduces a SIW feed exponentially tapered slot antenna for 60 GHz applications with a bandwidth of 0.8 GHz and a gain of 10 dBi.

In this article, a venus slot with SIW for enhancing the bandwidth was introduced, which has a bandwidth of 5.5 GHz. It is best suited to operate in short range and unlicensed applications and also in the materials used for construction in a Rogers substrate with a thickness of 0.381 mm. The electromagnetic tool is used to simulate the proposed antenna, tested, and validated the results like reflection coefficient, that is, voltage standing wave ratio (VSWR). The impedance equivalent model is introduced to match the reflection coefficient and MATLAB software is used to analyze the performance.

## 1 | INTRODUCTION

The worldwide spectrum of 60 GHz is available in the literature,<sup>1–4</sup> and it is presented in Figure 1. This frequency

## 2 | SIW-VENUS SLOT ANTENNA

The SIW is invented for high-frequency applications that are millimeter-wave applications and its nature is similar to a

waveguide. The dominant mode is TE<sub>10</sub> and states that two rows of vias were integrated with both top and flip side ground planes via a substrate. The spacing (*s*) and diameter (*d*) of holes or vias play the key role in the design of SIW and

the used conditions are  $d \leq \frac{\lambda_g}{5}$  and  $s \leq 2d$ .<sup>7–12</sup> The standard equation used to calculate the width of SIW is

$$a_R = a_{SIW} - \frac{d^2}{0.95s} \quad (1)$$

The diameter (*d*) to a width of waveguide (*a<sub>R</sub>*) is not mentioned in Equation (1)<sup>11,12</sup> and sometimes it will give error values and the more appropriate equation is represented as

$$a_{SIW} = a_R + 1.08 \times \frac{d^2}{s} - 0.1 \times \frac{d^2}{a_{SIW}} \quad (2)$$

The generalized procedure to develop a slot is shown in Figure 2, and the proposed slot antenna is presented in Figure 3, where Figure 3A,B shows the top side and the flip view. The design printed with an RT Duriod 5880 material,  $\epsilon_r = 2.2$  (Rogers substrate), with a 0.381-mm-thickness substrate and microstrip feed are used.

The dimension of the antenna is 13 mm × 9 mm × 0.381 mm and the Venus-shaped slot is etched on the top side of the substrate. The top, bottom views of a fabricated prototype is shown in Figure 4, and the parameters used in the design are *W* = 13 mm, *L* = 9 mm, *D*<sub>2</sub> = 1 mm, *S* = 0.6 mm, *D* = 0.3 mm, *D*<sub>3</sub> = 0.55, *D*<sub>4</sub> = 1.1, *W*<sub>1</sub> = 0.84 mm, *W*<sub>2</sub> = 2.6 mm, *W*<sub>3</sub> = 2 mm, *W*<sub>4</sub> = 0.2 mm, *W*<sub>5</sub> = 4.755 mm, *W*<sub>s</sub> = 3.09 mm, *L*<sub>1</sub> = 7.3 mm, *L*<sub>2</sub> = 0.85 mm, *L*<sub>3</sub> = 0.85 mm, *L*<sub>4</sub> = 0.89 mm, *L*<sub>5</sub> = 0.87 mm, and *L*<sub>6</sub> = 1.75 mm.

### 3 | RESULTS AND DISCUSSION

The reflection coefficient of a proposed design is represented in Figure 5 and the frequency observed was in between 57 GHz and 64 GHz. The impedance bandwidth is around 5.5 GHz with a reference of −10 dB line. The impedance bandwidth ranges from 57 GHz to 62.48 GHz with a

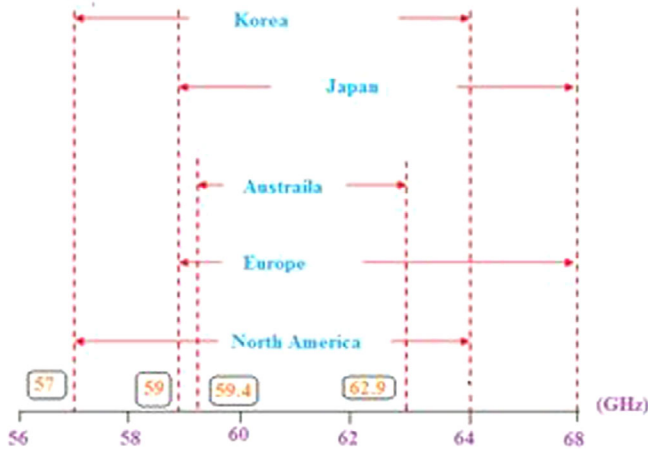


**FIGURE 1** Worldwide spectrum available for 60 GHz [Color figure can be viewed at [wileyonlinelibrary.com](http://wileyonlinelibrary.com)]

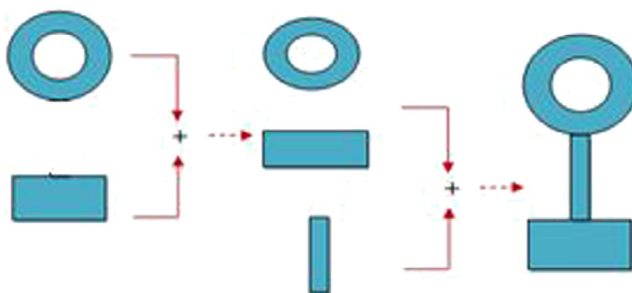


**FIGURE 2** Geometry of Venus shaped [Color figure can be viewed at [wileyonlinelibrary.com](http://wileyonlinelibrary.com)]

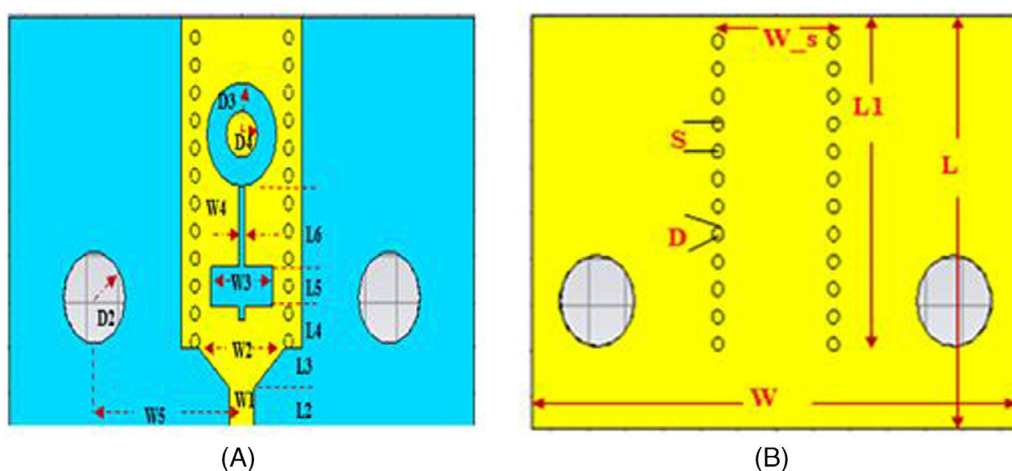


**FIGURE 3** Venus-shaped SIW slot antenna. A, Top view. B, Bottom view. SIW, substrate-integrated waveguide [Color figure can be viewed at [wileyonlinelibrary.com](http://wileyonlinelibrary.com)]

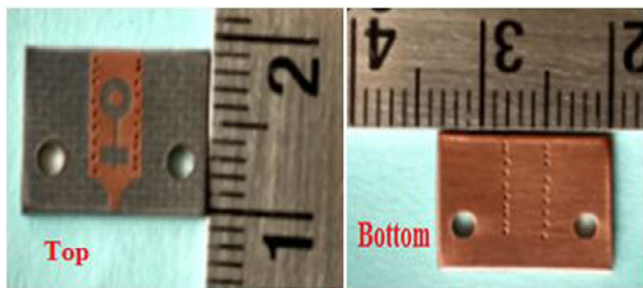


**FIGURE 4** Fabricated prototype [Color figure can be viewed at [wileyonlinelibrary.com](http://wileyonlinelibrary.com)]

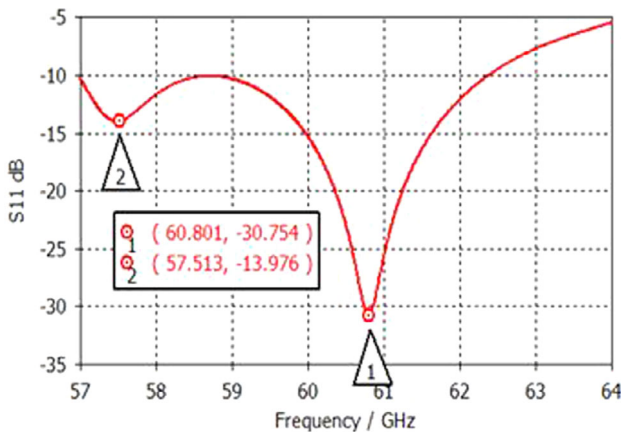


**FIGURE 5** Reflection coefficient over frequency (GHz) [Color figure can be viewed at [wileyonlinelibrary.com](http://wileyonlinelibrary.com)]

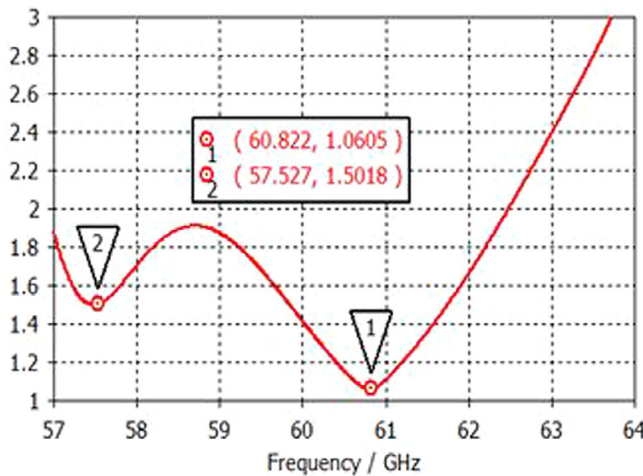


**FIGURE 6** VSWR for the proposed design. VSWR, voltage standing wave ratio [Color figure can be viewed at [wileyonlinelibrary.com](http://wileyonlinelibrary.com)]

reference of  $-10$  dB line and produces two resonant frequencies of  $57.5$  GHz and  $60.8$  GHz, and their  $S_{11}$  values are  $-14$  dB and  $30.75$  dB.

The VSWR over a frequency of the proposed design is demonstrated in Figure 6 and a frequency band range of  $57$ – $64$  GHz was observed. This also has a bandwidth

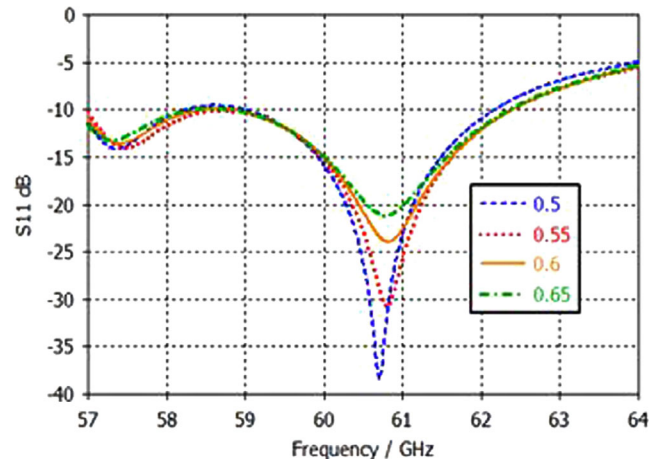


**FIGURE 7**  $S_{11}$  values for different values of  $D_4$  [Color figure can be viewed at [wileyonlinelibrary.com](http://wileyonlinelibrary.com)]

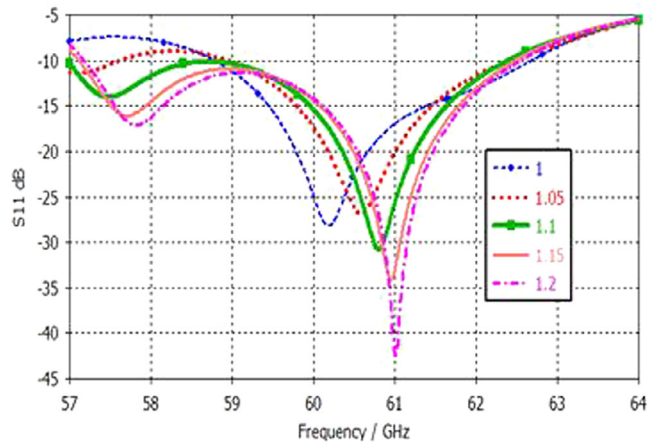


**FIGURE 8**  $S_{11}$  values for different values of  $D_3$  [Color figure can be viewed at [wileyonlinelibrary.com](http://wileyonlinelibrary.com)]

of around  $5.5$  GHz with reference to  $\text{VSWR} = 2$  line and matches with the impedance bandwidth of this design. The  $\text{VSWR}$  values are  $1.5$  at  $57.5$  GHz and  $1.06$  at  $60.82$  GHz. The  $S_{11}$  values for different values of inner circle radius are shown in Figure 7 and represented the parameter as  $D_4$ , and five values were considered for analyzing the  $S_{11}$  and their values are  $0.5$  mm,  $0.55$  mm,  $0.6$  mm, and  $0.65$  mm. With the increase of the  $D_4$  values, the resonant frequency increases and the reflection coefficient value decreases, but there is no effect on bandwidth.

The  $S_{11}$  results for different values of  $D_3$  are represented in Figure 8 and five values were considered for analyzing the performance, which were  $1$  mm,  $1.05$  mm,  $1.1$  mm,  $1.15$  mm, and  $1.2$  mm. The change in  $D_3$  will affect bandwidth, reflection coefficient, and resonant frequency. If  $D_3$  increases, then the bandwidth will increase and the condition used for  $D_3$  is given as follows:

$$\frac{\lambda}{4} \leq 2 \times D_3 \leq \frac{\lambda}{2} \quad (3)$$

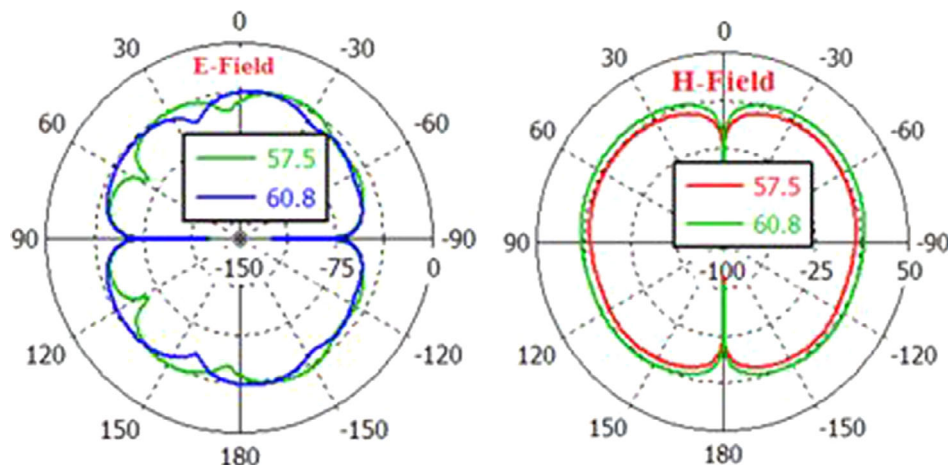


**FIGURE 9** Radiation patterns [Color figure can be viewed at [wileyonlinelibrary.com](http://wileyonlinelibrary.com)]

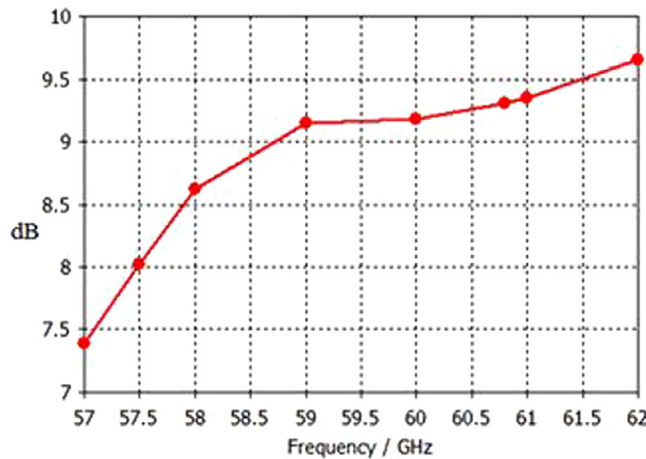


**FIGURE 10** Proposed antenna gain. A, 57.5 GHz. B, 60.8 GHz  
[Color figure can be viewed at [wileyonlinelibrary.com](http://wileyonlinelibrary.com)]

The E-field and H-field patterns of the proposed design at two resonant frequencies are presented in Figure 9, and bidirectional radiation and stable patterns were observed and well suited for wireless applications.

The maximum gain over frequency is represented in Figure 10. The gain values of the proposed designs are 7.4 dBi at 57 GHz, 8 dBi at 57.5 GHz, 8.6 dBi at 58 GHz, 9.15 dBi at 59 GHz, 9.2 dBi at 60 GHz, 9.35 dBi at 60.8 GHz, 9.37 dBi at 61 GHz, and 9.65 dBi at 62 GHz. The surface current distribution of a proposed antenna is presented in Figure 11 at two resonant frequencies of 57.5 GHz and 60.8 GHz, and revealed that the flow of current is more at starting and ending of the slot. Table 1 is the comparison of proposed design with the existing size of antenna, gain, bandwidth, and dielectric constant. The proposed design has more bandwidth, less size and average gain compared with the existing structures.

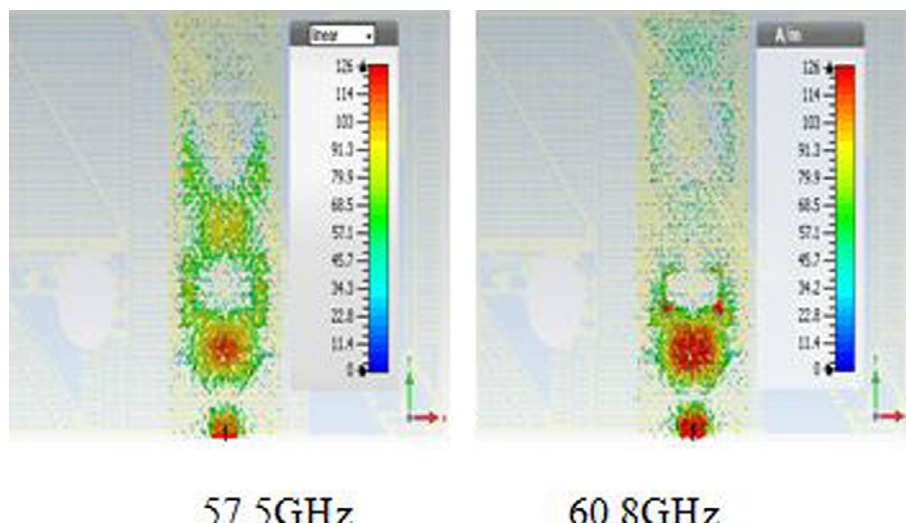


**FIGURE 11** Surface current distributions [Color figure can be viewed at [wileyonlinelibrary.com](http://wileyonlinelibrary.com)]

**TABLE 1** Comparison with the existing literature

Ref.	Antenna size (mm <sup>3</sup> )	Dielectric constant	Gain (dBi)	Bandwidth (GHz)
1	14 × 16 × 2.6424	$\epsilon_r = 2.2$	14.8	1.1
	22 × 24 × 2.624		16.8	2.8
3	34 × 24.75 × 0.85	$\epsilon_r = 2.2$	21.6	1.1
4	25 × 16 × 0.635	$\epsilon_r = 2.2$	6	3
5	44.61 × 9.93 × 0.381	$\epsilon_r = 2.2$	13.7	3
6	33.5 × 8 × 0.787	$\epsilon_r = 2.2$	10	0.8
Proposed	15 × 10.7 × 0.381	$\epsilon_r = 2.2$	9	5.1

**TABLE 2** Comparison of simulated and measured results

S. No.	Method	Resonant frequency (GHz)	Reflection coefficient (dB)	VSWR
1	SR	57.513	-13.976	1.501
	MR	57.77	-15.35	1.43
2	SR	60.801	-30.754	1.605
	MR	60	-29.6	1.073

Abbreviation: VSWR, voltage standing wave ratio.

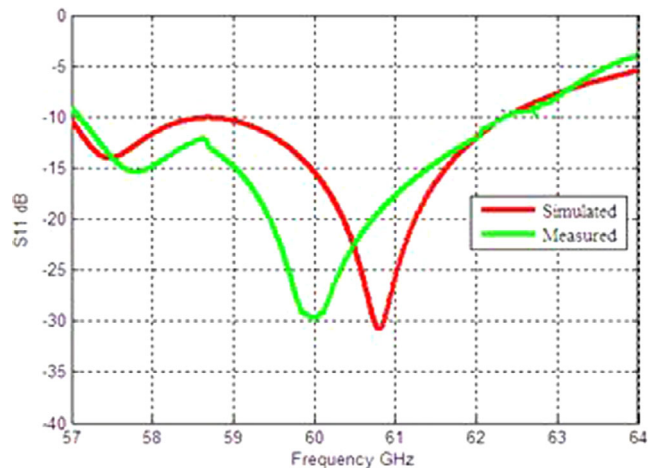


**FIGURE 12**  $S_{11}$  values for simulated and measured results [Color figure can be viewed at wileyonlinelibrary.com]

Comparisons of simulated and measured reflection coefficients and VSWRs are presented in Figures 12 and 13, and a small variation is observed in the measured results when compared with simulation results due to small fluctuations in the creation of holes in the fabricated prototype (spacing and diameter of vias are very small). The simulation and measured impedance bandwidth ranges are 9.29% and 9.21%, and the measured bandwidth ranges from 57.15 GHz to 62.45 GHz with two resonant frequencies of 57.77 GHz and 60 GHz. Table 2 shows a clear comparison of simulation and measured results where SR and MR are simulated and measured results.

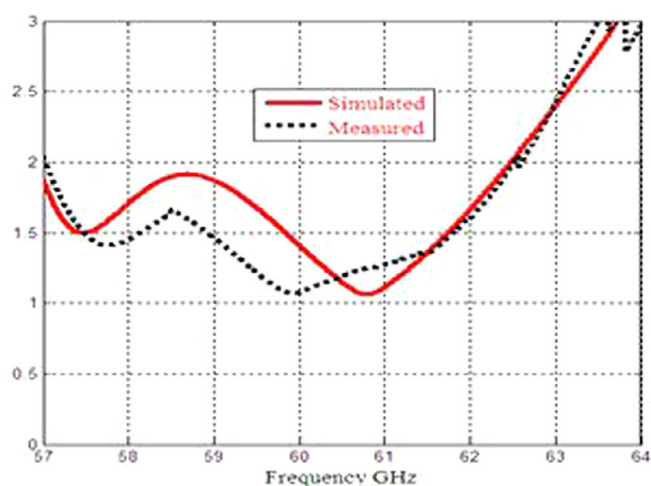


**FIGURE 13** VSWRs for simulated and measured results. VSWR, voltage standing wave ratio [Color figure can be viewed at wileyonlinelibrary.com]

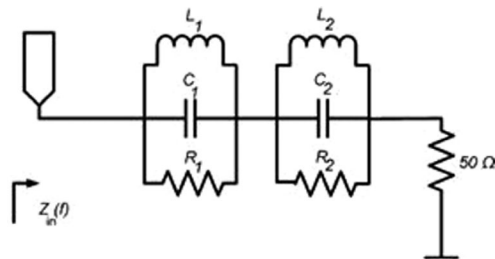


**FIGURE 14** RLC equivalent circuit model ( $R_1 = 15 \Omega$ ,  $R_2 = 32 \Omega$ ,  $L_1 = 1.1094 \text{ pH}$ ,  $L_2 = 1.9857 \text{ pH}$ ,  $C_1 = 6.912 \mu\text{F}$ , and  $C_2 = 1.9857 \mu\text{F}$ )

## 4 | EQUIVALENT CIRCUIT MODEL

The RLC equivalent circuit model for proposed antennas is shown in Figure 14, and the first circuit will generate a resonant frequency of 57.77 GHz and the second circuit will resonate at a frequency of 60.8 GHz. The equivalent model is to equate the proposed antenna reflection coefficient and the steps are given as follows:

1. Observe the simulation results (reflection coefficient).

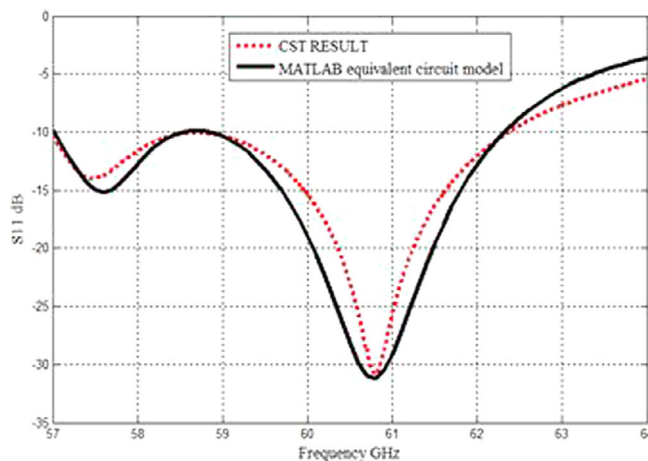


**FIGURE 15** Reflection coefficient [Color figure can be viewed at wileyonlinelibrary.com]

2. Calculate R,L,C values by using the standard formulas.<sup>10</sup>
3. Find the input impedance of the circuit using the transfer function method.
4. Find the VSWR value with the help of formulae.
5. Convert VSWR into  $S_{11}$  values and plot the graph vs frequency.
6. Compare with simulation results to validate the RLC equivalent model.
7. If it is valid stop the process, otherwise change R,L,C values and repeat the procedure step 2 to step 6.

The RLC model is developed by MATLAB for analyzing the reflection coefficient of the proposed design. Figure 15 describes that the frequency vs  $S_{11}$  simulated value of reflection coefficient of  $-30.754$  dB for an RLC equivalent circuit model with MATLAB and CST results, and by comparing two results, the proposed parallel RLC equivalent circuit model is acceptable and also matched with each other.

## 5 | CONCLUSION

A compact broadband SIW venus-shaped slot antenna was invented for V-band applications and fabricated prototype with a impedance bandwidth of 5.3 GHz, ranging from 57.15 GHz to 62.45 GHz and resonates at 57.8 GHz ( $S_{11} = -15.35$  dB), 60GHz ( $S_{11} = -29.6$  dB). The simulated and measured percentage impedance bandwidth ranges are 9.29% and 9.21%, and an RLC equivalent model is invented to match the reflection coefficient of a proposed antenna with the help of transfer function using the MATLAB software. The proposed antenna is useful for short-range applications such as WLAN, WPAN, automotive applications, and Gi-Fi.

## ACKNOWLEDGMENTS

The author's gratitude to MEITY Scheme (Visvesvaraya PhD Fellowship) for their financial support to do the research work.

## ORCID

Nanda Kumar Mungaru <https://orcid.org/0000-0001-6967-6859>

Shanmuganantham Thangavelu <https://orcid.org/0000-0002-2025-3844>

## REFERENCES

- [1] Bakhtafrooz A, Borji A. Novel two-layer MMW slot-array antennas based on substrate-integrated-waveguides. *Progress Electromagn Res*. 2010;109:475-491.
- [2] Li Y, Luk K-M. Low cost high gain and broadband substrate integrated waveguide fed patch antenna array for 60-GHz band. *IEEE Trans Antennas Propag*. 2014;62:5531-5538.
- [3] Tomas M, Lacik J, Puskely J, Raida Z. Design of aperture coupled microstrip patch antenna array fed by SIW for 60 GHz band. *IET Microw Antennas Propag*. 2016;10:288-292.
- [4] Gong K, Chen ZN, Qing X, Chen P, Hong W. Substrate integrated waveguide cavity-backed wide slot antenna for 60-GHz bands. *IEEE Trans Antennas Propag*. 2012;60:6023-6026.
- [5] Shrivastava P, Rama Rao T. 60 GHz radio link characteristic studies in hallway environment using antipodal linear tapered slot antenna. *IET Microw Antennas Propag*. 2015;9:1793-1802.
- [6] Ramesh S, Rao TR. Planar high gain dielectric loaded exponentially TSA for millimeter wave wireless communications. *Wireless Press Commun*. 2015;84:3179-3192.
- [7] Bozzi M, Georgiadis A, Wu K. Review of substrate integrated waveguide circuits and antennas. *IET Microw Antennas Propag*. 2011;5:909-920.
- [8] Cai Y, Zhang Y, Ding C, Qian Z. A wideband multilayer substrate integrated waveguide cavity backed slot antenna array. *IEEE Trans Antennas Propag*. 2017;65:3465-3473.
- [9] Zhang Z, Cao X, Gao J, Li S, Han J. Broadband SIW cavity-backed slot antenna for endfire applications. *IEEE Trans Antennas Propag*. 2018;17:1271-1275.
- [10] Nanda Kumar M, Shanmuganantham T. Division shaped substrate integrated waveguide slot antenna for millimeter wireless-/automotive radar applications. *J Comput Elect Eng*. 2018;71: 667-675.
- [11] Nanda Kumar M, Shanmuganantham T. Broad-band H-spaced head shaped slot with SIW based antenna for 60 GHz wireless communication applications. *Microw Opt Technol Lett*. 2019.
- [12] Nanda Kumar M, Shanmuganantham T. Substrate integrated waveguide based slot antenna for 60 GHz wireless applications. *Microw Opt Technol Lett*. 2019.

**How to cite this article:** Mungaru NK, Thangavelu S. Broadband substrate-integrated waveguide venus-shaped slot antenna for V-band applications. *Microw Opt Technol Lett*. 2019;1–6. <https://doi.org/10.1002/mop.31904>



# Design and Performance of Textile Antenna for Wearable Applications

S. Ashok Kumar<sup>1</sup> · T. Shanmuganantham<sup>2</sup>

Received: 20 February 2018 / Revised: 22 May 2018 / Accepted: 22 May 2018  
© The Korean Institute of Electrical and Electronic Material Engineers 2018

## Abstract

In this paper, a novel co-planar waveguide fed textile antenna is to be designed for wearable applications. The designed antenna has the design parameters of the size is  $90\text{ mm} \times 70\text{ mm} \times 1.57\text{ mm}^3$  and the substrate is Jeans cloth whose dielectric constant is 1.6. The proposed antenna resonates at 2.45 GHz with a return loss of  $-19\text{ dB}$ . The proposed antenna has a gain of 2 dBi and VSWR is around 1.1 at the resonating frequency. This logo shaped antenna can be radically used in military jackets, because of its compatibility, flexibility in structure design and shape, excellent performance at different angles, human safety, miniaturization, power consumption etc.

**Keywords** Wearable antenna · Textile antenna · Defence · Secure communication · Coplanar waveguide and etc.

## 1 Introduction

Textile antennas are found to have more significance in today's world in various fields of communication. The main aim of textile antennas is to be easily integrated with clothes. They are manufactured of conductive threads and yarn of conductive textile materials. The main challenges connected to textile antennas are the technology and materials for antenna manufacturing, the interaction between the antenna and top of human body, and the interaction between the antenna and environment [1].

Textile antennas are the main type of antennas used in wearable applications. Common textiles as cotton, denim, fleece, etc. can be used as dielectric substrates. Also polymer based materials are considered as possible substrates as they are robust, elastic and waterproof. The conductive part of the wearable antenna should share the same characteristics as everyday clothes, i.e. to be comfortable, unobtrusive, washable, elastic in all directions, etc. [2]. All of these demands can be met by embroidering or weaving conductive threads or yarn in textiles making the antenna a truly integral part of clothes [3–5]. Conductive threads can be thin solid metal wires or metal-plated polymer fibers. The textile antenna

operates in the proximity of human body which is a lossy dielectric. Part of the radiated power is absorbed in human body which reduces the antenna radiation efficiency and gain. On the other hand, the user is exposed to electromagnetic waves which can have adverse health effects if exposure limits are not observed [6]. Wearable antennas can be optimized for on-body operation (where the propagation along the body surface is desired) and off-body operation (where the EM wave should be launched in free space) [7]. When worn on the body, the antenna is subject to mechanical deformations such as bending, stretching or crumpling, which needs to be taken into account in the antenna design [8]. Wearable antennas are often required to work in harsh environments (rain, heat, snow, etc.), especially if military forces are considered. The presence of moisture in textile substrate severely affects the antenna radiation properties. The typical strategy to mitigate the influence of harsh environment is application of suitable waterproof textile substrates or antenna covers [9, 10].

In this paper, most of the outdoor clothing and equipment will have been layered with a Teflon protector by their manufacturers. This fabric protector is a coating that provides protection to clothing and equipment against stains, mud and liquids, without impacting upon the performance, feel or look of the item. The idea of having Teflon as a substrate in the antenna design is mainly due to the benefits it is provided with. The benefits are the fabric dries quickly when wet makes it easy to clean liquids and soil away repels water by beading up liquids allowing it to roll off makes

✉ S. Ashok Kumar  
ashokape@gmail.com

<sup>1</sup> Jothishamathi Institute of Technological Sciences,  
Hyderabad 505481, India

<sup>2</sup> Pondicherry University, Pondicherry 605014, India

the clothing and equipment more durable gives long lasting protection from dust, soil and stains.

## 2 Antenna Design Parameters

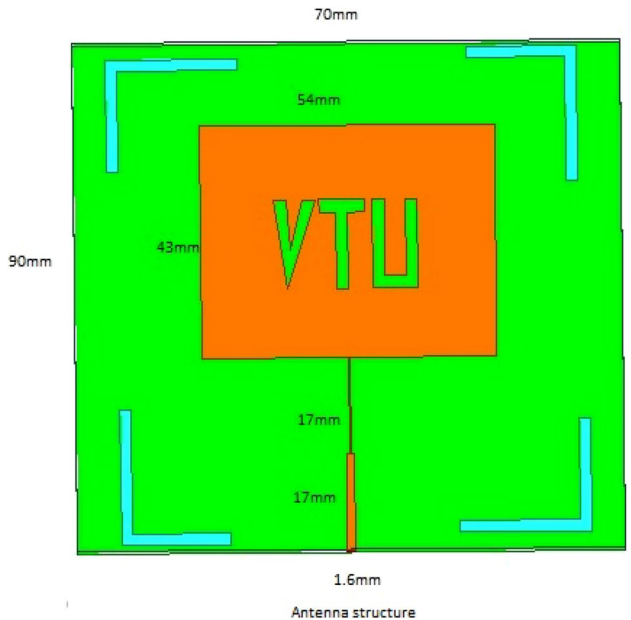
As this antenna is a wearable type, performance at different bending angles must be considered. Antenna bending may bring difference in antenna performance. In this attempt, the logo antenna for wearable applications shows compact size, lower return loss and electrical properties of cloth material. In this a logo antenna containing our university name is introduced and it is surrounded by fine copper embroidery. In wearable antenna we need to curb wave decline in complex human–environment. It is necessary to pay more attention in miniaturization than all other parameters. Full-wave optimization is required for the design of antenna and Low Noise Amplifier to meet the desired specifications. This structure is mainly for 2.45 GHz ISM band for wearable applications, because it reduces the human body attenuated signals.

This work represents an embroidered logo antenna is resonating in the resonant frequency at 2.45 GHz. It should be valuable for wearable application, the textile antenna is printed on jeans fabric of permittivity 1.6 and the radiating element is copper and we used capacitive coupling to print logo.

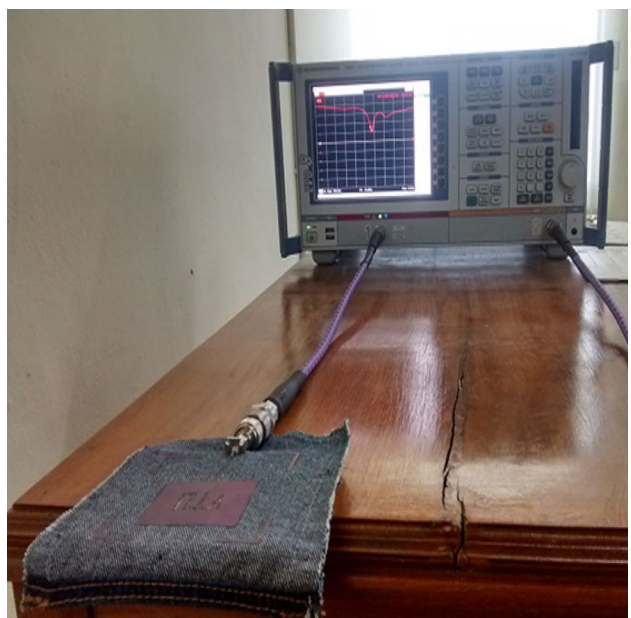
The proposed antenna structure comprises a path fed by a micro strip and ground path to decrease the radiation effect from body. The proposed structure has ground plane at the entire bottom surface reduces the radiation effect on human body. In this structure logo ‘VTU’ is carved on the radiating patch by using the principle of capacitive coupling. The radiating element is surrounded on four sides by fine copper thread embroidery. The performance of micro strip antenna depends on its dimensions such as width (W) and length (L).

Figure 1 shows the geometrical view of textile antenna for wearable applications at ISM band. The substrate used is Jeans fabric of permittivity 1.6. In this antenna structure dimensions are 90 mm × 70mm with thickness of 62 mils. The ground and radiator are made of copper with a thickness of 60 microns. A  $50\ \Omega$  micro strip feed of width 1.6 mm and length of 17 mm is used as antenna feed.

This antenna structure is designed and simulated by HFSS tool. The substrate for this antenna is denim fabric which is of 1.57 mm thickness. The simulated output produces a return loss or S11 parameter of about – 19 dB, this proves that antenna is about 94% efficient. The antenna structure is fabricated on jeans fabric of thickness 1.57 mm and permittivity of 1.6. As ground plane of this antenna structure is fully extended on the other side of the substrate, this antenna would be good enough to be used on human body. In this a pocket shaped jeans substrate is used. The fabricated structure is tested using vector network analyzer at CUSAT laboratory. The fabricated structure is shown in Fig. 2.



**Fig. 1** Geometrical view of proposed antenna



**Fig. 2** Prototype model of textile antenna

## 3 Results and Discussion

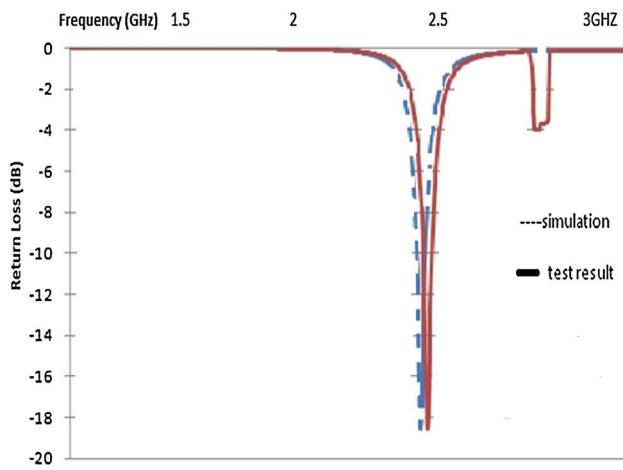
The design and analysis of textile antenna is performed using mentor graphics IE3D simulator. The optimized antenna design with the dimensions and its performance was validated.

Figure 2 shows the experimental measurement setup of textile antenna. In this measurement, the dipole has an effect

on demonstrating the polarization of the antenna. By altering the angle of the dipole, the polarization of the proposed antenna can be well verified.

A return loss S11 characteristic of textile antenna is shown in Fig. 3. Return loss of an antenna should be less than  $-10$  dB. The proposed antenna covers the range frequency between 2.1 and 2.6 GHz with the s-parameter shows less than  $-10$  dB. Higher the return loss lower will be interferences between the signals i.e., reflection is small, so that performance will be better. The maximum return loss around  $-28$  dB at 2.45 GHz frequency.

The polarization of the logo antenna working at textile antenna performs well in spite of the angles as shown in Fig. 4. In all, we can achieve the good performance of the polarization at same. The surface current distribution and



**Fig. 3** Return loss characteristics

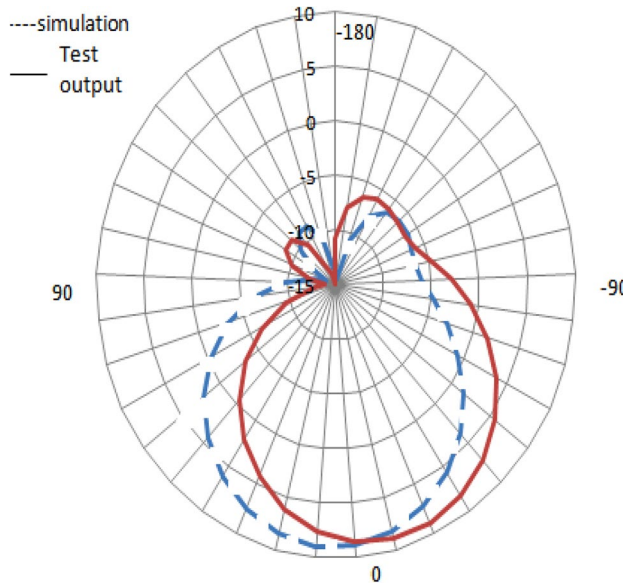


**Fig. 4** Radiation pattern XY plane

the radiation pattern at the frequency 2.45 GHz is shown in Fig. 5.

However, the gain of the major lobes still remains identical at all bending situations. The elevation and azimuth pattern of the proposed system is shows the high gain value of 2dBi. So the proposed textile antenna is perfect candidate for wearable applications. The 3D view of the textile antenna is exhibited maximum radiation in Fig. 5a, b.

The gain of the proposed antenna is measured using radiation pattern measurement. It is observed from the graph, the gain of the antenna is almost constant throughout the resonant band frequency. It is also being noted that the gain energy value remains same.

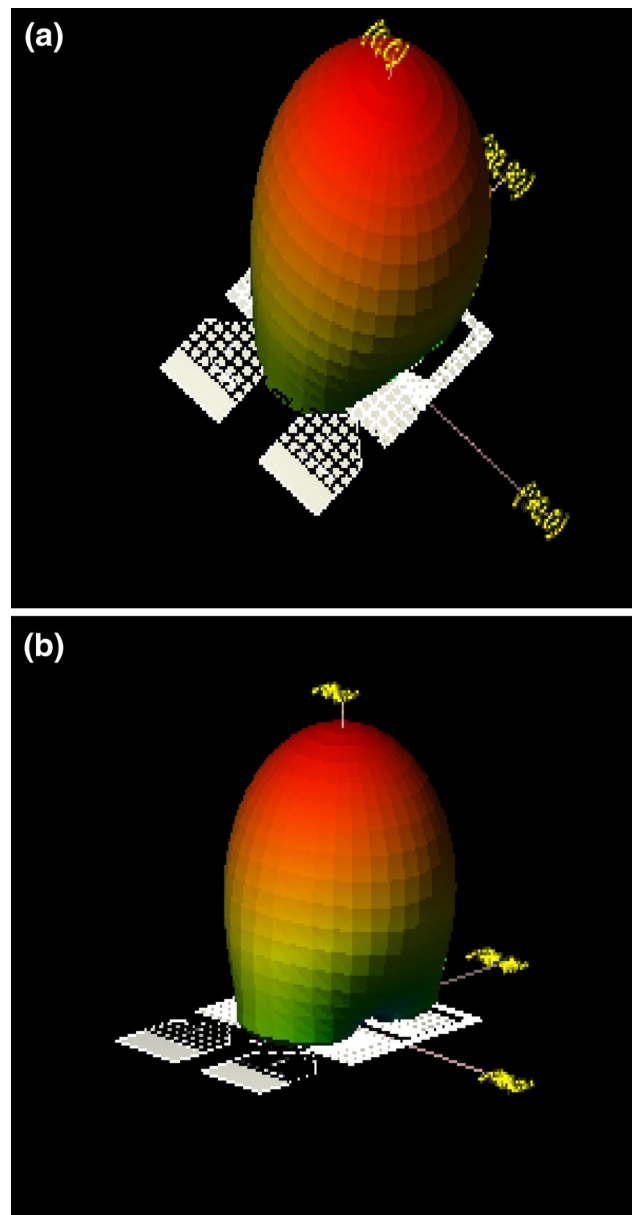


**Fig. 5** **a, b** 3D pattern of proposed antenna

## 4 Conclusion

A CPW fed textile antenna is designed for wearable applications at 2.45 GHz ISM Band frequency. The textile antenna was simulated and fabricated with jeans fabric substrate of dielectric constant is 1.6. From the results it is found that the structure has a better performance with a s11 of  $-19$  dB at the frequency of 2.45 GHz. This can be used for applications like military, border security forces & etc. Here the fabric used is jeans, since it is durable and is water proof easily gets rid of stains. It is very hard to design and fabricate the proposed antenna. The observed radiation patterns are stable within the frequency band.

## References

1. R. Sreelakshmy, S.A. Kumar, T. Shanmuganantham, A wearable type embroidered logo antenna at ISM band for military applications. *Micro. Opt. Tech. Lett.* **59**, 2159–2163 (2017)
2. S.A. Kumar, T. Shanmuganantham, Design and development of implantable CPW fed Monopole U slot antenna at 2.45 GHz ISM band for biomedical applications. *Microw. Opt. Tech. Lett.* **57**(7), 1604 (2015)
3. S. Izquierdo, J.C. Batchelor, M.I. Sobhy, Button antenna on textiles for WLAN on body application. *IET Micro. Ant. Prop.* **4**, 1980–1987 (2010)
4. T. Kellomäki, Analysis of circular polarization of cylindrically bent micro strip antennas. *Int. J. Antennas Propag.* **2012**, 1–8 (2012)
5. N Rais, P Soh, P Hall, *A Review of Wearable antenna. Lough Borough. International Conference*, pp. 120–126, 2009
6. S.A. Kumar, S. Thangavelu, Design and analysis of implantable CPW fed X-monopole antenna for ISM band applications. *Telmed. e- Health* **20**(3), 246 (2014)
7. S.A. Kumar, S. Thangavelu, CPW fed monopole implantable antenna for 2.45 GHz ISM band applications. *Inter. J Electron. Lett.* **3**(3), 152–159 (2015)
8. A. Talukder, D. Karmokar, K. Morshed, N. Mollah, Low profile inverted-F-L antenna for 5.5 GHz Wi MAX Applications. *ACEEE Int. J. Commun.* **3**, 12–19 (2012)
9. S.A. Kumar, S. Thangavelu, CPW fed implantable Z-Monopole antennas for ISM band biomedical applications. *Inter. J. Microw. Wirel. Tech.* **7**(5), 529–533 (2015)
10. H.Y. Chen, Y. Tao, Performance improvement of a U-slot patch antenna using a dual-band frequency selective surface with modified cross elements. *IEEE Trans. Antennas Propag.* **59**, 3482–3486 (2011)



## ORIGINAL ARTICLE

**Multiband SRR loaded Koch star fractal antenna**

C. Elavarasi\*, T. Shanmuganantham

*Dept. of Electronics Engg., School of Engg. and Tech., Pondicherry Central University, Pondicherry 605014, India*

Received 23 December 2016; accepted 1 April 2017

**KEYWORDS**

Coplanar waveguide [CPW];  
Koch star fractal;  
Multi band;  
Metamaterial [MTM];  
Negative permittivity/permeability;  
Circular split ring resonator [CSRR]

**Abstract** The Split ring resonator [SRR] loaded Koch star fractal antenna for multiple Freq band apps is presented. The CPW-Fed ant consists of Circular Split Ring Resonator [CSRR] which is fixed on reverse side of the substrate and iterated Koch star which is stamped on top of the FR4. The Koch fractal SRR antenna with a compacted size of  $12 \times 14 \text{ mm}^2$  is fabricated and tested. The multiple Freq for antenna measured capitulate with a  $-10 \text{ dB}$  at  $1.88/6.54/7.88/12.20/15.08 \text{ GHz}$  bands and cover up the Freq spectrum of GSM, WiMAX, IEEE 802.11a (WLAN)/b/g, IEEE 802.16e, ITU, S/C/X/Ku and K band, correspondingly. The extraction method of  $-ve$  permeability for the projected circular slit resonator is examined in detail. The antenna projected to have significant recompense, plus low profile, miniaturization capability with good S11 and VSWR is accepting for the functional frequency bands.

© 2017 Production and hosting by Elsevier B.V. on behalf of Faculty of Engineering, Alexandria University. This is an open access article under the CC BY-NC-ND license (<http://creativecommons.org/licenses/by-nc-nd/4.0/>).

**1. Introduction**

Multiple band ants occupy a chief part in current wireless communiqué systems. The essential antenna should be compacted, low cost/profile with impedance matching has to cover diverse functioning frequencies [1]. Distorted types of design provided for different user needs have been accounted in the literature. These existing designs have multifarious structures which create them complex to integrate with multiple functional band frequency. [Example: IEEE 802.11 g/b - (2.40 to 2.48), ISM - 2.4, IEEE 802.11 a for Wireless LAN - (5.15 to 5.35) and (5.750 to 5.825), RFID - 6.8, ITU - (8.02 to 8.5), IEEE 802.16 e for Wi-MAX - (3.40 to 3.69)] [2,3]. In wide ranging, multiple band resonating modes can be attained by altering

the radiating strip/ground flat and by utilizing dissimilar shapes. The employ of fractal conception and exploit of meta-materials usually confine the apps of the antenna owing to decreased complexity and miniaturized antenna dimension.

Meta-materials are non-natural materials that reveal both  $-ve$  permittivity/permeability Ppty's for the exact frequency regime. The SRR [split ring resonator] is a central edifice of meta-materials [4]. Abdelrehim and Ghafouri Shirazz employ MM lens by means of thin wire via CSRR [5]. Hema et al. offered the Novel Rectangular Ring Planar antennas considered for Ultra Wideband Apps (3.1 GHz towards 10.3 GHz) [2]. Dileep et al. made up Fractal loop based cylindrical dielectric resonator antenna for UWB. Elavarasi and Shanmuganantham have also reported in Ref. [7], that the fractal found in nature are irregular and made water-lily shaped patch antenna loaded with split ring resonator for multiple band operations. He-Xiu et al. reports CSRR fractal geometry achieves 1.1/2/2.74-band BPF/3D Gradient Index fractal Metamaterials worn for half Maxwell fish-eye lens antenna [8,9].

\* Corresponding author.

E-mail addresses: [celavarasi19@gmail.com](mailto:celavarasi19@gmail.com) (C. Elavarasi), [shanmugananthamster@gmail.com](mailto:shanmugananthamster@gmail.com) (T. Shanmuganantham).

Peer review under responsibility of Faculty of Engineering, Alexandria University.

In this article, Koch star fractal patch (Top Side) and SRR (Flipside) antenna are projected for IEEE 802.16 e [WiMAX] - 3.4 to 3.69 GHz, C band - 4.11 to 4.20 GHz, ITU and X band - 8.02 to 8.5 GHz/10.28 GHz, Ku band- 17.76 GHz. One of the most vital properties of fractals is self-similarity which is nothing but each iteration of Koch star has the equivalent shape as the complete Koch fractal [10]. CPW feed is used with source and symmetry ground. The SRR resonance frequency with permittivity characteristics of SRR is also calculated to validate the results. The superior performance of the antenna such as S11, gain, emission pattern and impedance bandwidth is mandatory to be roughly dependable by the entire operating frequency.

## 2. Antenna design

**Fig. 1(a)** shows the configuration of coplanar waveguide feed Koch star fractal patch antenna. The proposed Koch star fractal antenna is stamped on a Flame Retardant -4 substrate with dielectric constant  $\epsilon_r = 4.4$ . The Koch fractal patch is erected on the substrate whose dimensions are  $W \times L \times h \text{ mm}^3$  as exposed in the **Fig. 1(b)**. The antenna is fed by CPW consists of a 2 ground symmetry planes and source with the thickness of 1.6 mm. The Gap ‘g’ b/w the centre stripe and ground flat is 0.2 mm. The Koch star fractal patch configuration (top view) and circular split ring resonator (Reverse view) as publicized in the **Fig. 1(a)** and (b) along with the prototype of the SRR loaded Koch star are made to be known in the **Fig. 2** (a) and (b). The antenna planned proportions are shown in the **Table 1**.

## 3. Simulation results

The simulated results show fine agreement of multiple band operations of the proposed fractal antenna which ranges 2.10 /7.16/8.66/12.44/15.32/16.6 GHz with VSWR is at 1.023/1.25 1/1.28/1.26/1.32/1.56 which covers S/C/X/Ku band wide bandwidth from 11.78 GHz to 17.22 GHz which is useful for GSM/

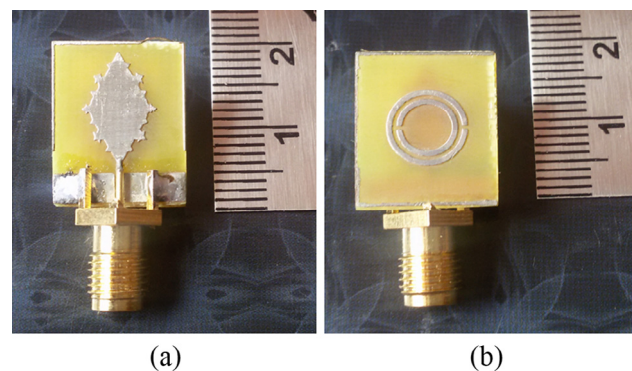


**Figure 2** Snap of the Fabricated SRR loaded Koch star fractal antenna Top and Flipside view.

**Table 1** Dimensions of Koch star fractal antenna demonstrated in **Fig. 1**.

Parameters	Value [mm]
$W/L/L_g/W_p/L_p/$	12/14/2.8/6.5/0.6/1.0
Gap/h/L <sub>1</sub>	0.2/1.6/3
$O_c/I_c/W_c/G_s$	4.5/3.5/0.3/0.3

IEEE 802.11/WLAN/IEEE 802.16/Wi-MAX applications as known in the **Fig. 1**.

To categorize with the behaviour of the ant's reverberating method, the made-up exciting current distributions of the antenna model are shown in the **Fig. 3**. For C band frequency, 4.0 GHz, current is principally practically in the feed line as revealed in **Fig 3(a)**. For the 8.0 GHz ITU with X band is in the area of the edging of the iterated Koch star fractal is given away in the **Fig. 3(b)**. For X band frequency 11.0 GHz the max. Current density is pragmatic in the Circular SRR as shown in the **Fig. 3(c)**.

The simulated gain of the SRR loaded Koch star fractal antenna has 3.71 dBi, 5.18 dBi, and 6.47 dBi at centre frequen-

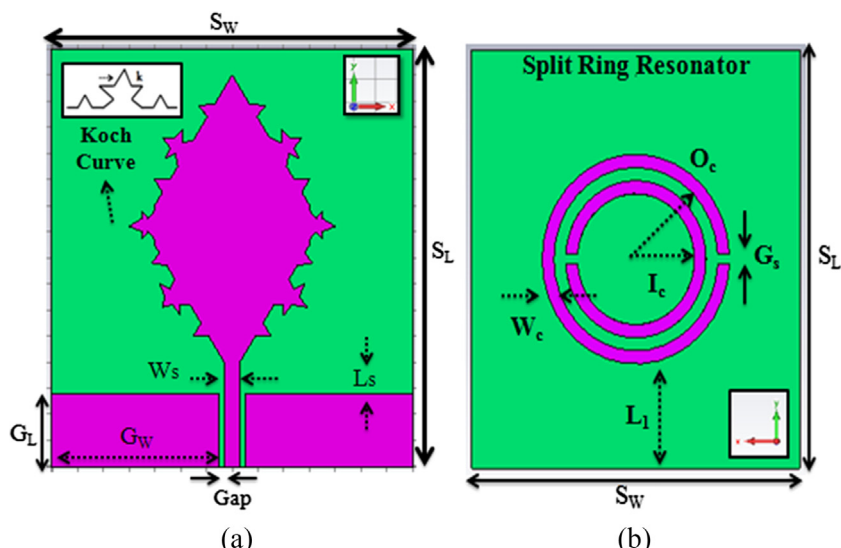


**Figure 1** Parameters of CPW Fed Koch fractal patch antenna [Top] and Construction of Circular SRR parameters [Bottom].

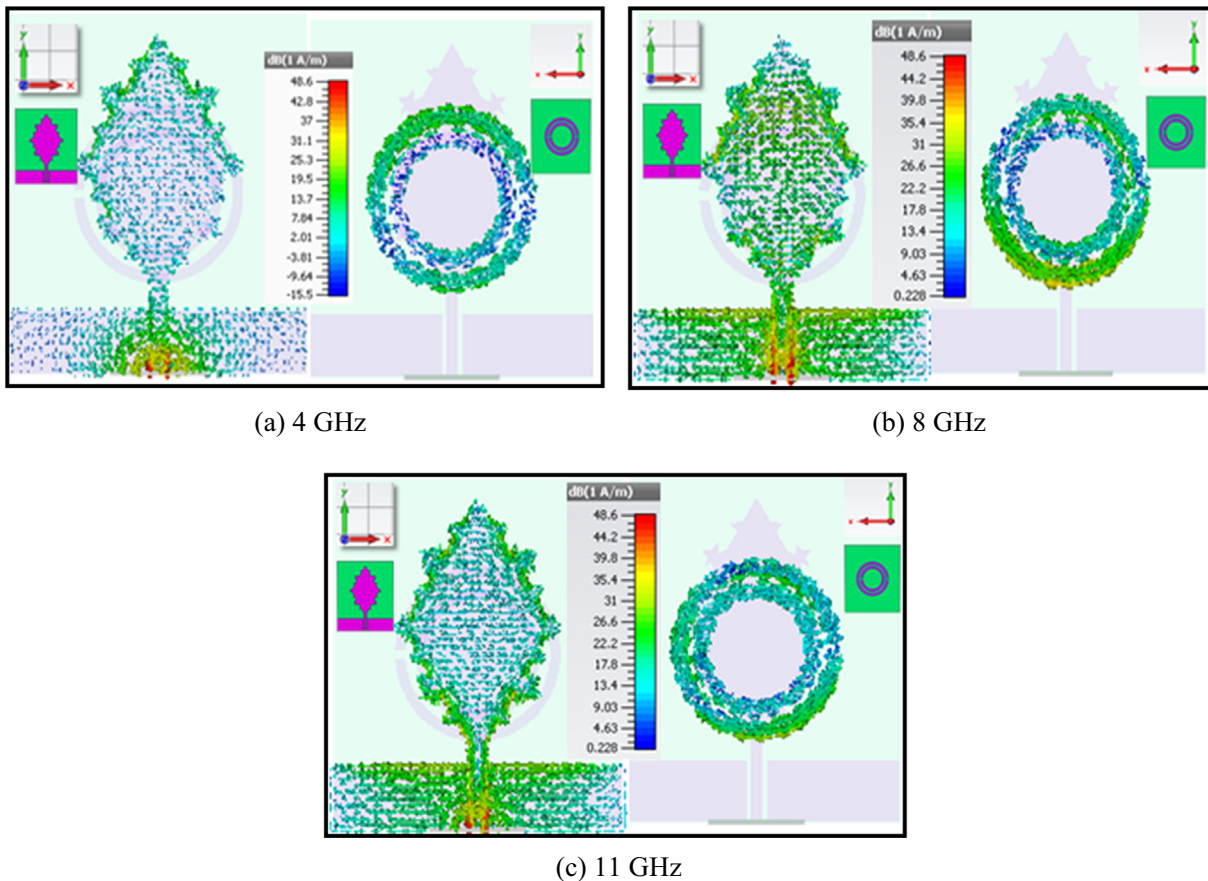


**Figure 3** Simulated surface current distributions for the antenna projected.

cies 6.0 GHz, 8.0 GHz and 11 GHz respectively. The Simulated gain in 3d Pattern is shown in the Fig. 4. Since Table 2, we can finish that the planned antenna produces superior performance in antenna proportions furthermore covering functional bands than the existing literatures.

#### 4. Parametric study

#### 4.1 Koch curve fractal

The formation of the curve is rather simple. A direct strip is mainly unfounded ready on three similar slices.

The centre, slice is a part furthermore restored via two sectors including the parallel span towards generating an equilateral  $\Delta\phi$ .

This progression is afterwards returning in favour of the four sectors producing next to the previous iteration, chief en route to the following plan in the 2nd iteration as given away in the Fig 5. Such a four side originator is pertained towards as the crow flies stroke directly to this

#### 4.1.1. Fractal dimensions

The fractal measurement is anxious away from the income of the Haus Dorff besicovitch equations and is being computed using Self-similar Pptv.

$$FD = \log[N]/\log[r] \quad (1)$$

Every part of the curve has the same on the whole quality than the sum total picture. The length and area of Koch curve are revealed in Table. 3. Precisely, Koch curve - Haus Dorff besicovitch equation confers, and put backs N via four (as the mutually monotone manner 4 sectors) along with r via three (as the portrayal practice agrees 4 fragments).

$$w_1(J, k) = \left[ \frac{1}{3}(J); \frac{1}{3}(k) \right] \quad (2)$$

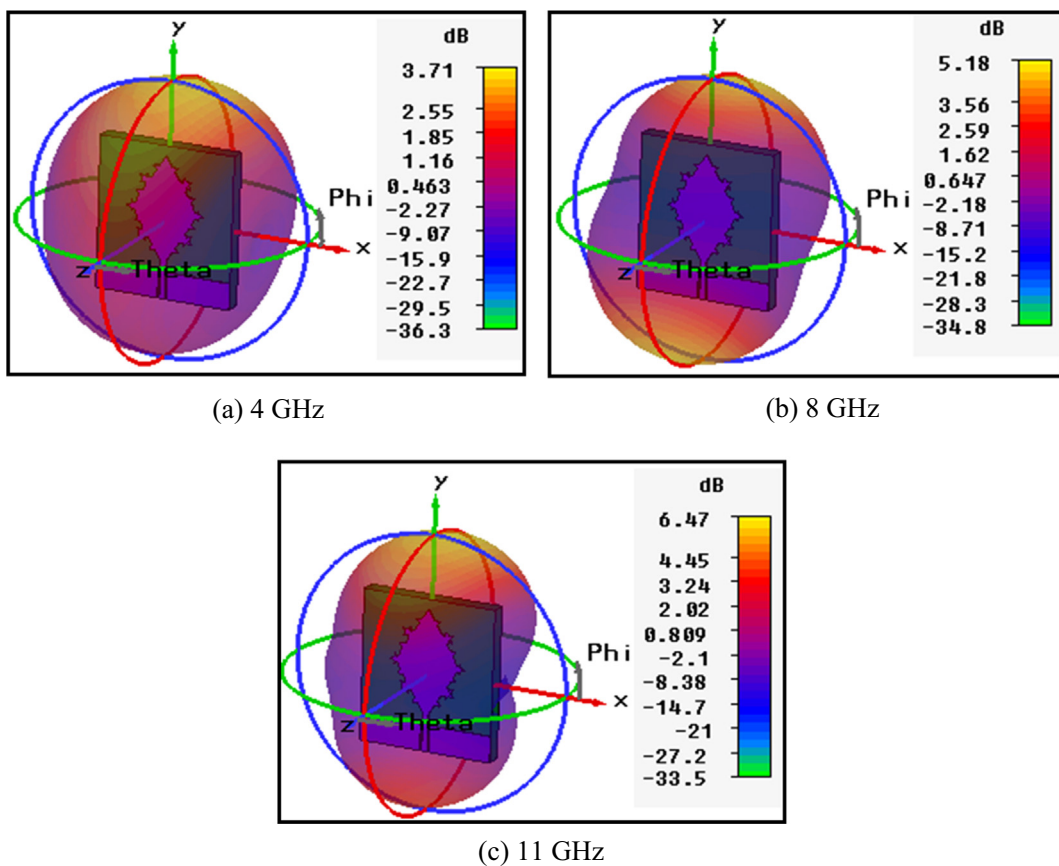
$$w_2(J, k) = \left[ \frac{1}{6}(J); \frac{\sqrt{3}}{6}(k) + \frac{1}{3}; \frac{\sqrt{3}}{6}(J) + \frac{1}{6}(k) \right] \quad (3)$$

$$w_3(J, k) = \left[ \frac{1}{6}(J); \frac{\sqrt{3}}{6}(k) + \frac{1}{2}; \frac{\sqrt{3}}{6}(J) + \frac{1}{6}(k) + \frac{\sqrt{3}}{6} \right] \quad (4)$$

$$w_4(J, k) = \left[ \frac{1}{3}(J) + \frac{2}{3}; \frac{1}{3}(k) \right] \quad (5)$$

42 SRR

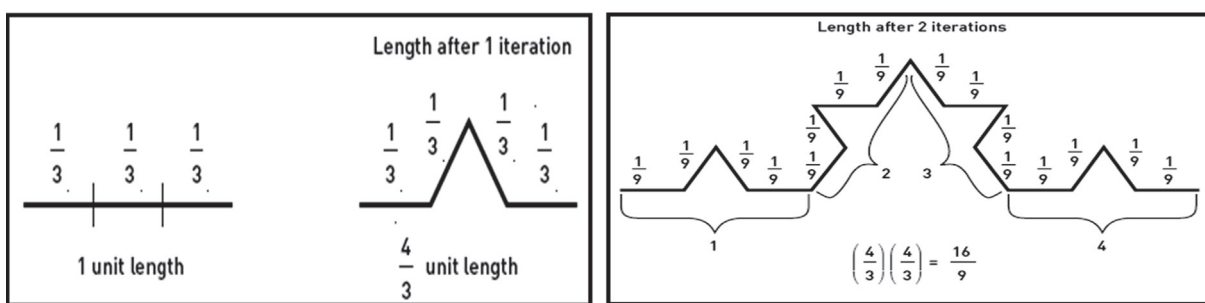
Pendry proposition about the NRI is nothing but the aim of an amalgamated material that is knowingly engineered to provide material properties that are not otherwise realistic with the usual materials. The negative permittivity and permeability from the S-parameters are recovered based on the effort of



**Figure 4** Simulated gain in 3d Pattern.

**Table 2** Comparison of different existing fractal MM antennas by way of antenna proposed.

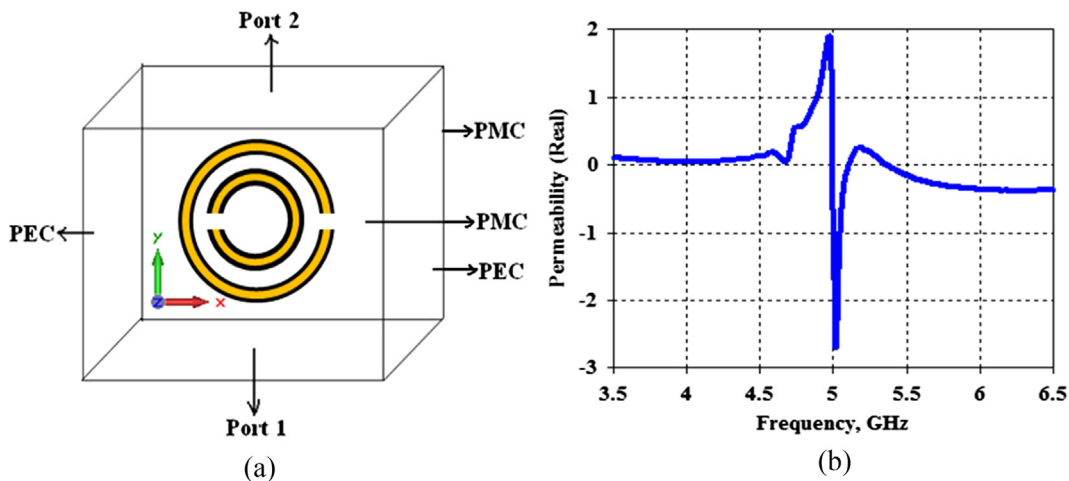
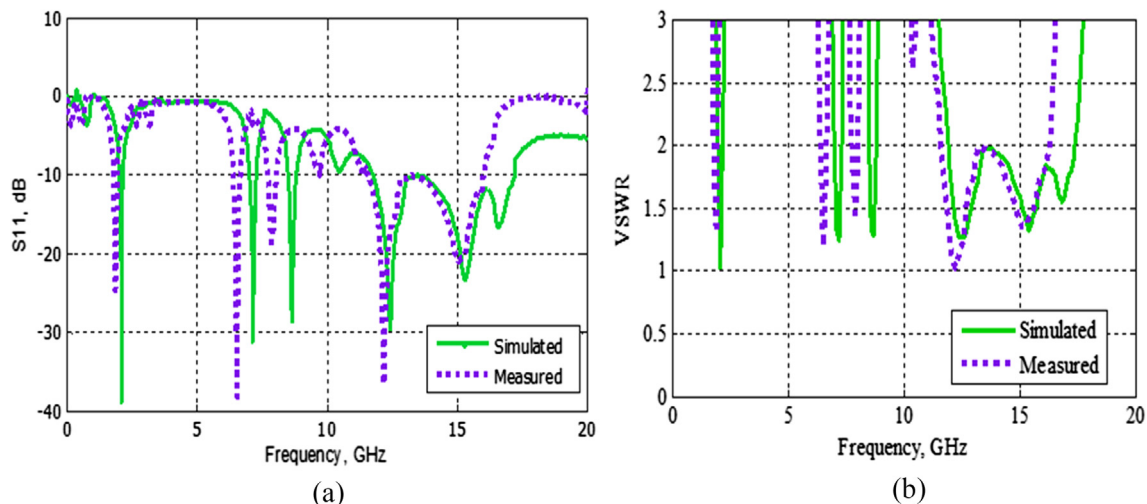
S. No.	References	Antenna size [mm <sup>2</sup> ]	Frequency [GHz] enclosed by antenna	Antenna nature
1.	Proposed	12 × 14	1.88/6.54/7.88/12.2/15.08	Multi-band
2.	[8]	14 × 16	3.8/8.68/13.96	Tri-band
3.	[2]	28 × 26	2.6/4.8	Dual-band
4.	[1]	40 × 40	2.5/5.5	Dual-band
5.	[3]	23 × 10.8	3.60	Single-Band
6.	[4]	14 × 14	1.780/3.520/5.260	Tri-band
7.	[6]	25.5 × 25.5	2.45/5.50	Dual-Band



**Figure 5** Iterations of KC fractal

**Table 3** Length and area of Koch star fractal.

Iteration	Calculating unit length	Koch star unit length	Curve area	Sector span	Curl length	$\Delta$ gle numeral	$\Delta$ gles area
0	1 unit $\times$ 1 unit	1	0.00	1.0	1.000	0.0	0.0
1	$\left[\frac{4}{3}\right]$	$\left[\frac{4}{3}\right]$	1.00	1/3.0	1.320	1.0	1.0
2	$\left[\frac{4}{3}\right] \times \left[\frac{4}{3}\right]$	$\left[\frac{16}{9}\right]$	1.44444	1/9.0	1.760	4.0	0.445
3	$\left[\frac{4}{3}\right] \times \left[\frac{4}{3}\right] \times \left[\frac{4}{3}\right]$	$\left[\frac{4}{3}\right]^3$	1.64197	1/27.0	2.360	16.0	0.195
4	etc.	etc.	etc.	etc.	etc.	etc.	etc.

**Figure 6** Waveguide setup for CSRR.**Figure 7** S11/VSWR of SRR loaded Koch star fractal antenna.

Smith et al. The circular split ring resonator has average ring lengths as eq.,

$$RL_{CSRR1} = 2\pi x r_{CSRR1} - S_{CSRR1} \quad (6)$$

$$RL_{CSRR2} = 2\pi x r_{CSRR2} - S_{CSRR2} \quad (7)$$

The SRR usually consists of two clanging rings engraved on dielectric substrates along with their constantly comprise gaps lying on opposing sides. They employ in favour of assembling

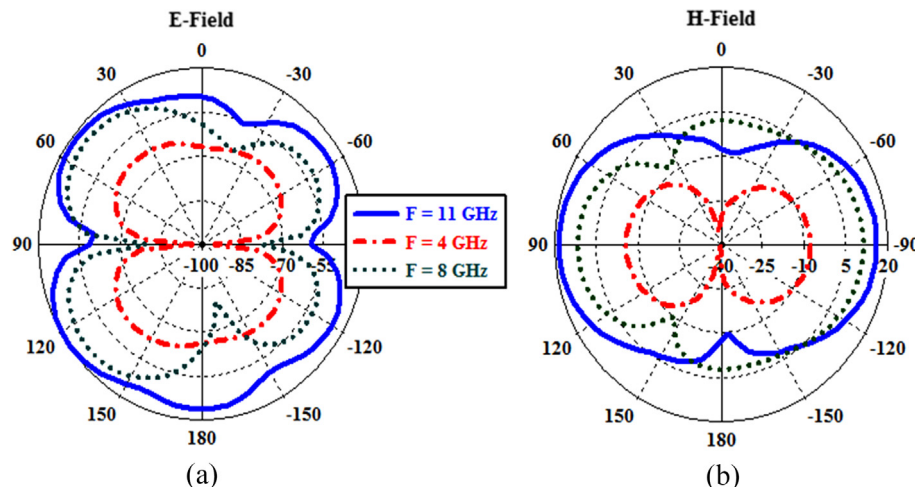
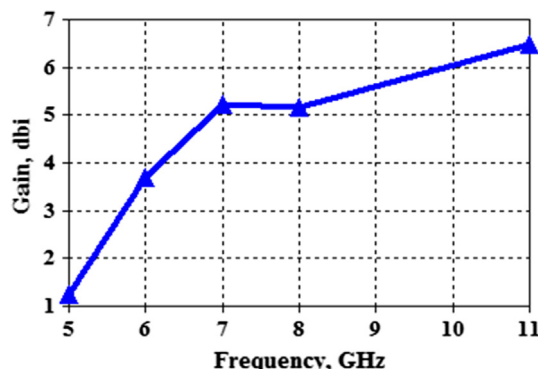
left handed media with negative refractive index. The resonance frequency of both circles occurs at the same wavelength ( $\lambda_g/2$ ) as eqn.,

$$Rf_{CSRR1} = \frac{c_{CSRR1}}{2L_{CSRR1}\sqrt{\epsilon_{eff}}} \quad (8)$$

$$Rf_{CSRR2} = \frac{c_{CSRR2}}{2L_{CSRR2}\sqrt{\epsilon_{eff}}} \quad (9)$$

**Table 4** Simulated and measured parameters.

S.No.	Frequency (GHz)		Reflection coefficient (dB)		VSWR	
	SV	MV	SV	MV	SV	MV
1	2.10	1.88	-38.70	-24.70	1.023	1.293
2	7.16	6.54	-31.22	-38.22	1.251	1.207
3	8.66	7.88	-28.51	-18.51	1.280	1.458
4	12.44	12.20	-29.57	-36.51	1.260	1.034
5	15.32	15.08	-23.32	-20.87	1.320	1.350
6	16.60	-	-16.65	-	1.560	-

**Figure 8** Far-field pattern for antenna projected (4.0/8.0/11.0 GHz).**Figure 9** Measured peak gain.

## 5. Extraction of negative permeability

In this revision, the Nicolson Ross Wier process is measured to attain the negative permeability of the proposed circular-SRR antenna. The proposed CSRR structure is validated with the -ve permeability characteristics, waveguide method are worn to describe. The proposed circular Split Ring structure is placed within waveguide as open in the Fig. 6(a). The CSRR intention to create, -ve permeability is experiential for a resonant frequency at 5 GHz where the SRR multiple band Koch star frac-

tal antenna design has exposed notch in the S11 characteristics. The real parts of permeability are extracted as given away in Fig. 6(b). Thus, effective material constraints extract the best manner to prove the realism of meta-material Ppty.

## 6. Measured results

The measured results show superior agreement of multiple band operations of the SRR loaded Koch star fractal antenna which ranges 1.88/6.54/7.88/12.2/15.08 GHz with VSWR is at 1.293/1.207/1.458/1.034/1.35 which covers L/C/Ku band with wide bandwidth from 11.56 GHz to 16.02 GHz which is useful for GSM/IEEE 802.11/WLAN/IEEE 802.16/Wi-MAX applications as exposed in the Fig. 7(a). The VSWR is tested to be below 2 characters as exposed in the Fig. 7(b). The simulated/measured antenna parameters are made known in the Table 4.

The measured radiation outline of the planned split ring resonator Koch star fractal antenna is demonstrated in Fig. 8(a) and (b). It shows the E (theta/phi) and H (theta/phi) of the antenna proposed at the resonant frequencies 4.0 GHz, 8.0 GHz and 11.0 GHz, correspondingly. The measured rate of recurrence is made known in Fig. 9. It is capable of exist to smooth the progress of the radiation model in the far field, which authorizes fine monopoly similar energy features in extra of the functioning Freq band.

## 7. Conclusion

In this manuscript, coplanar waveguide fed SRR loaded Koch star Fractal antenna is obtainable, which has 1.88 GHz at  $-24.70$  dB covering L band, 6.54 GHz at  $-38.22/7.88$  GHz at  $-18.51$  covering C band, and 12.20 GHz at  $-36.51/15.08$  GHz at  $-20.87$  covering Ku band applications. Fractal meta-material antenna consists of compact size ( $12 \times 14$  mm $^2$ ) which is for multioperating frequencies. A prototype of the projected antenna is fabricated plus tested. These multiple band antennas can be smoothly integrated by the printed circuit boards (PCBs) of wireless Communication devices. Subsequently, we can carry out fine L, C, X and Ku bands with magnifications of SRR loaded Koch star fractal antenna.

## References

- [1] Mohammad Sadegh Sedghi, Mohammad Naser-Moghadasi, Ferdows B. Zarraabi, A dual band fractal slit antenna loaded by jerusalem crosses for wireless plus WiMAX communications, *Prog. Electro-magnet. Res. Lett.* 61 (2016) 19–24.
- [2] Hemachandra Reddy Gorlaa, Frances J. Haracki-ewicz, A novel rectangular circle planar monopole ant for ultra wide-band application, *Prog. Electro. Magnet. Res. C* 61 (2016) 65–73.
- [3] N. Mishra, R.K. Chaudhary, A miniaturized ZOR antenna with enhanced bandwidth for WiMAX applications, *Microw. Opt. Tech. Lett.* 58 (1) (2016) 71–75.
- [4] Payam Beigi, Pejman Mohammadi, A novel small triple-band monopole antenna with crinkle fractal-structure, *Int. J. Electron. Commun.* 70 (2016) 1382–1387 (Elsevier AEU).
- [5] A.A. Adel Abdelrehim, Hooshang Ghafouri Shirazz, Performance improvement of patch antenna using circular split ring resonators and thin wires employing metamaterials lens, *Progr. Electro. Magn. Res. B* 69 (2016) 137–155.
- [6] Susilo Ady Saputro, Jae-Young Chung, Hilbert curve fractal antenna for dual on- and off-body communication, *Prog. Electro Magnet. Res. Lett.* 58 (2016) 81–88.
- [7] C. Elavarasi, T. Shanmuganantham, Parametric analysis of water lily shaped SRR loaded fractal monopole antenna for multiband application, *WASET Int J Electr. Comp. Energetic Electro Comm. Eng.* 10 (9) (2016).
- [8] Xu He-xiu, Wang Guang-ming, Peng Qing, Liang Jian-gang, Novel design of triple-band band pass filter based on fractal shaped geometry of a complementary single split ring resonator, *Int. J. Electr. Tay France* 98 (5) (2011) 647–654.
- [9] He-Xiu Xu, Guang-Ming Wang, Zui Tao, Tong Cai, An octave bandwidth half maxwell fish eye lens antenna using 3D gradient -index fractal metamaterials, *IEEE Trans Ant Propaga.* 62 (39) (2014).
- [10] R. Poonkuzhal, Zachariah C. Alex, T. Baala krishnan, Miniaturized wearable fractal-antenna for military application at VHF-band, *Prog. Electro-magn. Res. C* 62 (2016) 179–190.



# Design and analysis of implantable CPW fed bowtie antenna for ISM band applications



S. Ashok Kumar\*, T. Shanmuganantham

*Department of Electronics Engineering, Pondicherry University, Pondicherry, India*

## ARTICLE INFO

### Article history:

Received 13 May 2013

Accepted 6 August 2013

### Keywords:

Biomedical applications

Implanted antenna

ISM band

Method of moments and coplanar waveguide feed

## ABSTRACT

A novel implantable coplanar waveguide (CPW) fed crossed bowtie antenna is proposed for short-range biomedical applications. The antenna is designed to resonate at 2.45 GHz, one of the industrial-scientific-medical (ISM) bands. It is investigated by use of the method of moments design equations and its simulation software (IE3D version 15). The size of the antenna is 371.8 mm<sup>3</sup> (26 mm × 22 mm × 0.65 mm). The simulated and analyzed return losses are –23 and –25 dB at the resonant frequency of 2.45 GHz. We have analyzed some more performances of the proposed antenna and the results show that the proposed antenna is a perfect candidate for implantation. The proposed antenna has substantial merits like low profile, miniaturization, lower return loss and better impedance matching with high gain over other implanted antennas.

© 2013 Elsevier GmbH. All rights reserved.

## 1. Introduction

Implantable antennas are gradually becoming the focus of research, in which the wireless link acts as a vital role in the communications between the medical implants and external devices. This results in the implantation of medical devices inside the human body for the purpose of monitoring which in turn can be extended to controlling certain human biological parameters [1,2]. To quote a few of those, it includes simple pulse monitors, motion monitors, and portable holter monitors. The Medical Implant Communications Service (MICS) has allocated the band of 402–405 MHz for bio medical applications [3,4]. A healthcare provider can set a wireless link between an implanted device and a base station so as to allow a high speed reliable system to monitor the health conditions of the patient in real time [5]. Even a wireless endoscopy is possible using these systems. Compared with the conventional endoscopy method, wireless tablet endoscopy affords a direct study of the entire small intestine and does not require any sedation [6]. Past one decade, the works of implantable antennas are in the form of microstrip antenna or planar inverted-F antenna (PIFA), operating at single frequency band, which is 402–405 MHz [7].

In recent years, a dual-band implanted antenna has emerged. Lee et al. proposed a π-shape antenna with double L-strips operating at two closely spaced frequencies of 375 and 427 MHz to enhance the bandwidth [8]; Karacolak et al. proposed an antenna

with serpentine configuration operating at 402–405 MHz MICS band and 2.4–2.48 GHz Industrial, Scientific, and Medical (ISM) band [9]; Sánchez-Fernández et al. adopted a microstrip patch antenna based on short-circuited ring and spiral resonators, also operating at the MICS and ISM bands [10]. The design and realization of a 3D-spiral small antenna was also proposed at the MICS band [11]. Most recently, a triple-band implantable antenna was proposed, operating at 402 MHz, 433 MHz and 2.45 GHz [12]. Additionally, due to the size limitation of the implantable antennas, stacked structures were also adopted [11–13].

In this paper, the coplanar waveguide (CPW) fed crossed bowtie implantable antenna is proposed, which can be connected more easily with differential circuitries, eliminating the loss. The antenna operates at the frequency of 2.45 GHz, to work with a sub GHz wide-band transceiver designed for high-data rate implantable neural recording.

The organization of this paper is summarized as follows. In Section 2, the geometrical details of the proposed antenna are discussed. This follows Section 3, which details the operating principle of the implantable CPW fed antenna. This section also provides the proof that proposed antenna is much suitable for ISM band medical applications with its simulation and measured results. This is followed by conclusion remark in Section 4.

## 2. Geometrical view of proposed antenna

### 2.1. Biocompatibility

Most of the medical wireless applications for the human body, such as body area network and implanted devices are involved

\* Corresponding author. Tel.: +91 9750140862.

E-mail addresses: [ashokape@gmail.com](mailto:ashokape@gmail.com) (S.A. Kumar), [shanmuga.dee@pondiuni.edu.in](mailto:shanmuga.dee@pondiuni.edu.in) (T. Shanmuganantham).

**Table 1**

Dielectric properties of human tissues.

Tissue	Relative permittivity	Conductivity (S/m)
Muscle	$\epsilon_r = 52.7$	Sigma = 1.73
Skin	$\epsilon_r = 38$	Sigma = 1.46
Fat	$\epsilon_r = 5.28$	Sigma = 0.10
Bone	$\epsilon_r = 18.54$	Sigma = 0.80

in the electromagnetic coupling into and out of the human body. This coupling usually requires an antenna to transmit a signal into a body or pick up a signal from a body. The antenna operating environment for the implanted antenna is different from the traditional free-space communications, which is lossy environment. Designing an efficient implanted antenna is a key requirement in the direction of reliable medical implanted communication system. The implanted antenna must be long term biocompatible, possible to be embedded on existing implant device. The antenna must be electrically insulated from the body so as not to short out and be ineffective. Despite the fact that various types of miniature antennas and radiators have been developed, the literature on them is limited [14].

The most common miniaturization method used for preserving the biocompatibility of the antenna. Simultaneously separating the metal radiator from human tissue is to cover the structure with a superstrate dielectric layer [15]. Commonly used biocompatible materials include MACOR ( $\epsilon_r = 6.1$ ;  $\tan \delta = 0.005$ ) and Teflon ( $\epsilon_r = 2.1$ ,  $\tan \delta = 0.001$ ) [16]. But, it is important to emphasize that the substrates do not easily lend themselves to drilling and round cuts [17].

Insulating the implantable antenna with a thin layer of low loss biocompatible coating is another reported approach [18]. Materials proposed for biocompatible encapsulation include zirconia ( $\epsilon_r = 29$ ;  $\tan \delta = 0.0002$ ) [18] and PEEK ( $\epsilon_r = 3.2$ ;  $\tan \delta = 0.01$ ) [19]. On the basis of its electrical properties, alumina ceramic is a better substrate for biocompatible insulation from an electromagnetic point of view. High permittivity and low loss tangent values allow the near fields of the antenna to concentrate inside the low-loss encapsulation layer, thus mitigating power loss.

## 2.2. Design of antenna

A bowtie antenna is a wire approximation in two dimensions of a biconic dipole antenna. When used in planar configuration, it takes the form of a tapered, where the minimum and maximum distances between the slot edges correspond to its operating frequency range [20]. Using the triangular elements, bandwidth is greatly increased, to cover the entire ISM band. To improve the bowtie slot antenna, we replaced the straight sides of the tapered patch and opposite side tapered patch presented in [21] with a parabolic curve. Using this modified crossed bowtie antenna, we determined its ability to tune to the 2450 MHz ISM band. The top view of the antenna is shown in Fig. 1. The feeding structure of the crossed bow tie antenna consists of a coplanar waveguide (CPW) with  $50\Omega$  impedance. Matching the mode impedance of the CPW to  $50\Omega$  is obtained by tuning the distance between the tracks and as well as the width of the tracks as shown in Fig. 1.

The simulation model setup for the proposed antenna design is shown in Fig. 2. The values for each couple of dielectric values reported in Table 1 are valid at the specified frequency. The antenna was constructed on alumina ceramic substrate with thickness of 0.65 mm and dielectric constant  $\epsilon_r$  of 9.8 and implanted into muscle, skin, fat and bone with permittivity and conductivity as tabulated in Table 1 [18].

The equivalent transmission circuit for proposed antenna is shown in Fig. 3 and the structure is divided into five sections,

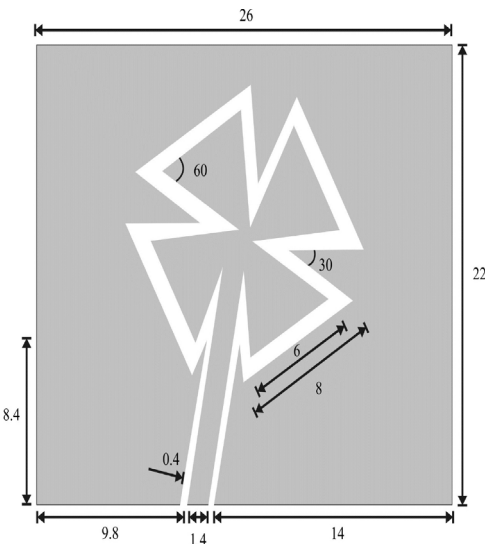


Fig. 1. Geometrical view of proposed antenna (all dimensions are in mm).

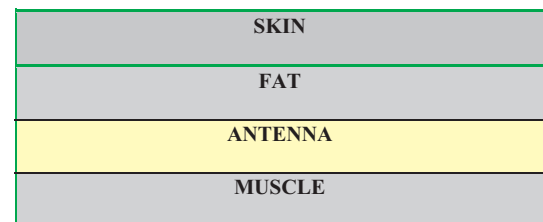


Fig. 2. Antenna simulated setup model.

where each section is considered as a separate transmission line of a defined length  $L$  and characteristic impedance  $z_0$ .

The characteristic impedance of the section can be expressed as,

$$z_0 = \frac{30\pi}{\sqrt{\epsilon_{eff}}} \frac{K(k')}{K(k)} \quad (1)$$

where  $k$  and  $k'$  are 1st kind of elliptical integrals, and  $\epsilon_{eff}$  is the effective dielectric constant of alumina ceramic substrate.

Solving the  $L$  and  $C$  coefficients using  $\pi$  and  $T$  network simplifications, finally got the simplest equivalent transmission model as shown in Fig. 4. Where  $z_1$  is the equivalent value for Sections I–III,  $z_2$  is the equivalent value for Sections IV and V. simplifying these circuit and find the input impedance  $Z_{in}$

$$Z_{in} = z_1 // z_2 // z_3 \quad (2)$$

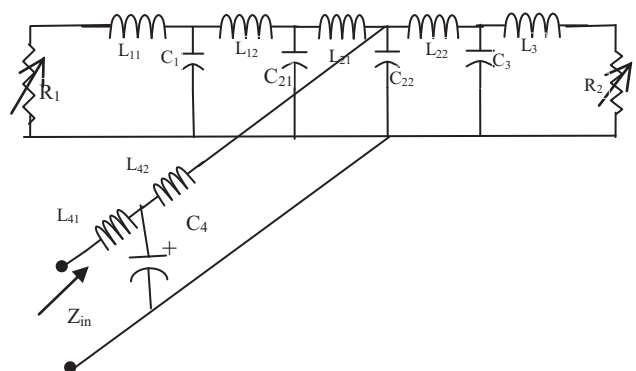
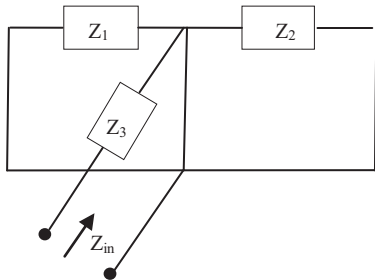
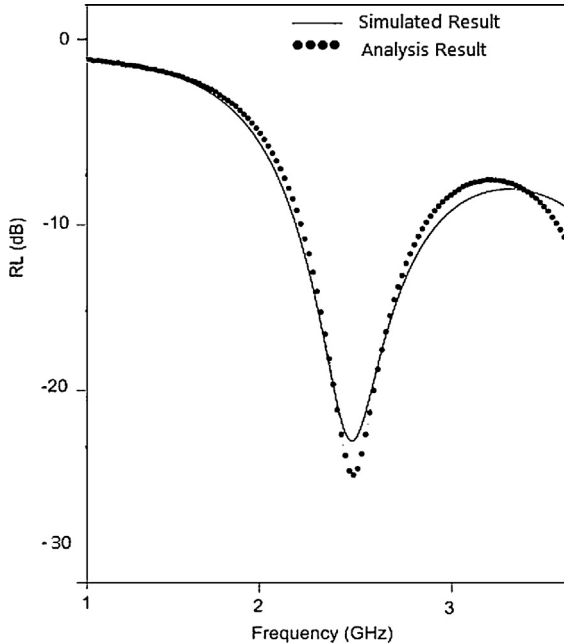


Fig. 3. Equivalent transmission line model for proposed antenna.



**Fig. 4.** Simplest equivalent transmission line model of Fig. 3.



**Fig. 5.** Return loss for simulation and analysis setup.

where  $z_1, z_2$  and  $z_3$  follows,

$$z_1 = z_2 = \frac{s^{20}L^8C^{12} + 4s^{18}L^7C^{11} + 84s^{16}L^6C^{10} + 271s^{14}L^5C^9 + 518s^{12}L^4C^8 + 612s^{10}L^3C^7 + 392s^8L^2C^6 + 96s^6LC^5}{s^{19}L^7C^{12} + 13s^{17}L^6C^{11} + 72s^{15}L^5C^{10} + 212s^{13}L^4C^9 + 376s^{11}L^3C^8 + 416s^9L^2C^7 + 256s^7LC^6 + 64s^5C^5} \quad (3)$$

$$z_3 = \frac{s^9L^3C^6 + 6s^7L^2C^5 + 12s^5LC^4 + 8s^3C^3}{s^{16}L^6C^{10} + 11s^{14}L^5C^9 + 50s^{12}L^4C^8 + 112s^{10}L^3C^7 + 152s^8L^2C^6 + 112s^6LC^5 + 32s^2C^2} \quad (4)$$

Using the values of input impedance, the reflection coefficient, VSWR, return loss and bandwidth can be computed using the following relations [22],

$$\text{Reflection coefficient, } k = \frac{z_{in} - z_0}{z_{in} + z_0} \quad (5)$$

$$\text{VSWR} = \frac{1 + |k|}{1 - |k|} \quad (6)$$

$$\text{Return loss} = 10 \log \frac{1}{k^2} = -20 \log(k) \quad (7)$$

where  $z_0$  is the characteristic impedance of the coplanar waveguide feed. Fig. 5 shows a comparison between the analyzed and simulated return loss of the antenna in planar state. The simulations are performed using the IE3D simulator Mentor Graphics and analysis results are performed using above equations.

Finally the numerical analysis operation is based on the flowchart as shown in Fig. 6. Algorithm for the design process is discussed in following steps.

### Algorithm.

- Step 1: Start the numerical solution for given proposed antenna.
- Step 2: Select the relative permittivity, loss tangent and thickness of the dielectric material.
- Step 3: Draw the equivalent transmission line model.
- Step 4: Solving the  $L$  and  $C$  coefficients, calculate input impedance using full wave analysis.
- Step 5: Calculate the S-parameter.
- Step 6: Check whether the S-parameter is matching or not; if matching stop the process, otherwise go with step 4.

### 3. Results and discussion

In real life scenario, the antenna is intended to be implanted into the human body, subcutaneously, particularly implanted inside the muscle fat skin tissue. Hence the measurement setup, using a human tissue is as follows. The antenna with human tissue is placed at the center of a plastic container of dimensions  $20\text{ cm} \times 20\text{ cm} \times 8\text{ cm}$  filled with one liter of human body liquid. This liquid mimics the dielectric characteristics of human muscle, fat and skin tissue at 2.45 GHz.

#### 3.1. Numerical results

The proposed implantable CPW fed crossed bowtie antenna is constructed into numerical analysis. The boundary mode analysis for the antenna is shown in Fig. 7. P1 and P2 regions are represents proposed antenna conducting region and ground region, respectively. Fig. 8 shows the contour region of bowtie antenna and it is represents a 2D analysis of a field, the contour lines have also been indicated. Such a representation gives a very good idea of what the field looks like in reality. A great deal with accurate and convenient representation of field on which all data referring to radiation can be plotted in Figs. 9 and 10.

#### 3.2. Experimental results

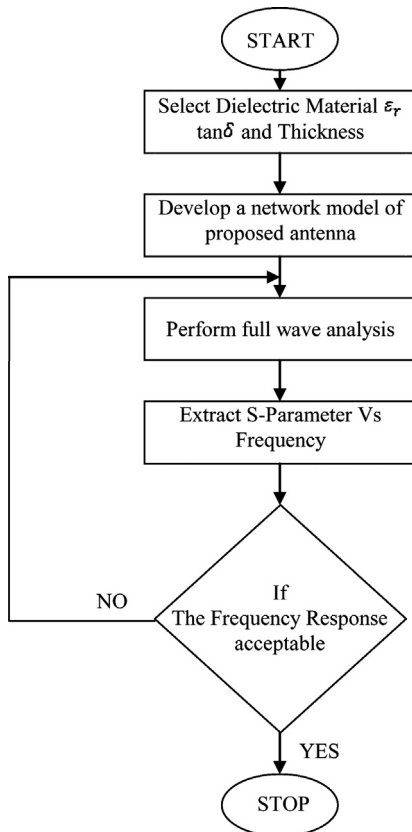
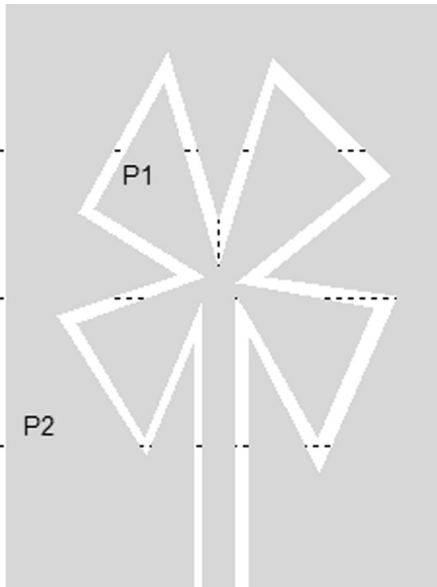
Experimental investigations are necessary in order to validate the numerical simulations for implantable CPW fed antennas. Since it is not possible to carry out measurements inside the human

---

body, investigations are performed by measuring laboratory, fabricated prototypes (Fig. 11) inside either tissue-equivalent mediums (phantoms).

##### 3.2.1. Prototype fabrication

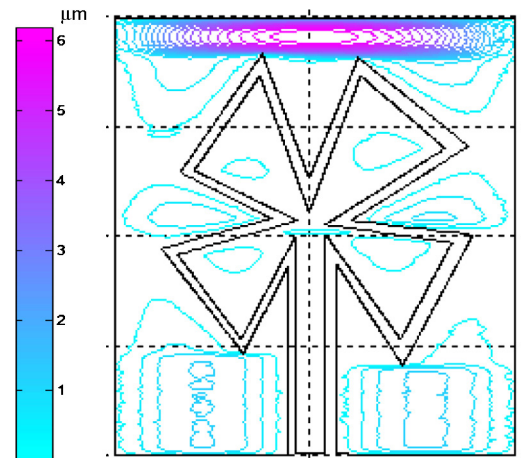
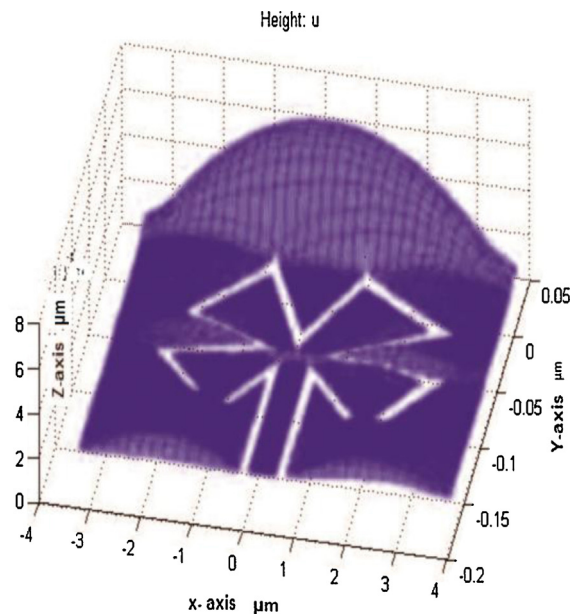
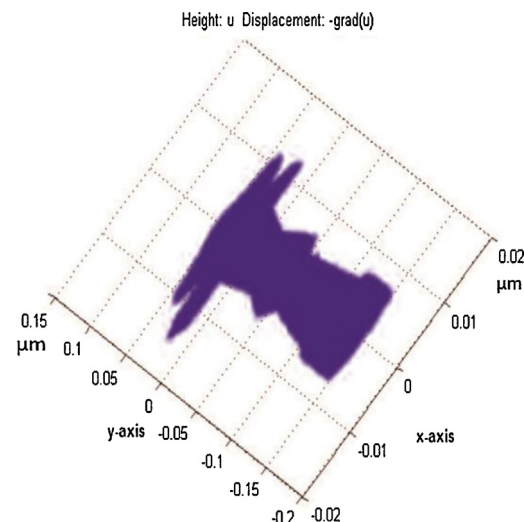
Due to the unavailability of biocompatible materials in some laboratories, we purchased biocompatible alumina ceramic material from alibaba manufacturer, china. Prototype fabrication of implantable antennas meets all classical difficulties of miniature antennas. The coplanar waveguide feed used to connect the antenna with the network analyzer may give rise to radiating currents on the outer part of the cable, which, in turn, deteriorate measurements (Fig. 12). The effects of different feeding techniques for implantable patch antennas were analyzed in [22]. Bowtie antenna prototypes immersed inside phantoms, with the ground plane being in direct contact with the tissue-emulating material, were found to be insignificantly influenced by the coaxial cable. Based on the above, the numerical antenna

**Fig. 6.** Flowchart for design process.**Fig. 7.** Boundary model of proposed antenna.

model must be slightly adjusted in order to take prototype fabrication considerations into account. Example fabricated prototypes of implantable antenna is shown in Fig. 11. Numerical simulations and experimental measurements must be carried out with the exact same antenna structure in order to be able to validate the design.

### 3.2.2. Testing inside phantoms

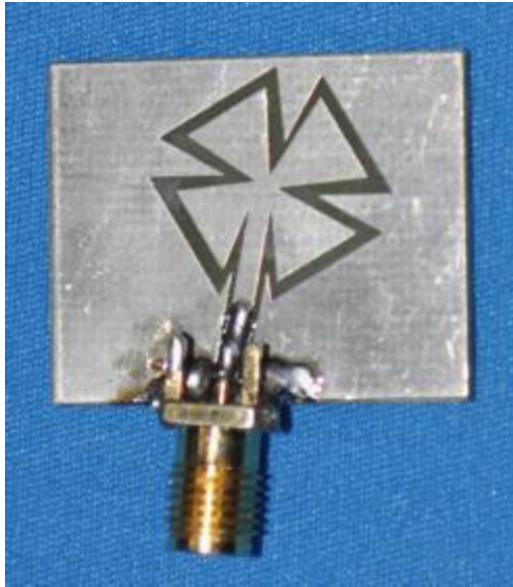
Testing inside phantoms are relatively easy and practical to implement. The fabricated prototype is immersed inside a tissue

**Fig. 8.** Contour region of proposed antenna.**Fig. 9.** Top view of proposed antenna radiation.**Fig. 10.** Radiation view of proposed antenna.

**Table 2**

Phantoms used for testing of implantable antennas.

Tissue	Shape	State	Ingredients	Relative permittivity	References
Skin	Rectangular	Gel	Deionized water, Sugar, agarose	$\epsilon_r = 38$	[7]
Scalp	Rectangular	Gel	Water, salt, acrylamide, TMEDA, ammonium per sulphate	$\epsilon_r = 28$	[20]
Rat tissue	Rectangular	Gel	Deionized water, DGBE, Triton X-100	$\epsilon_r = 45.2$	[14]
Skin	Rectangular	Gel	Deionized water, sugar deionized water, salt, vegetable oil, flour deionized water, sugar, salt	$\epsilon_r = 38$	[16]
Muscle				$\epsilon_r = 52.7$	
Fat				$\epsilon_r = 5.28$	

**Fig. 11.** Fabrication of proposed antenna.**Fig. 12.** Photograph of measurement setup model.

phantom and measured. For validation purposes, the same scenario as that of the numerical simulations has to be considered. Canonically-shaped phantoms have so far been used for testing implantable antennas. In this case, the main challenge lies in the formulation and characterization of tissue-emulating materials. Example phantoms and tissue recipes reported in the literature are given in Table 2 [7,20,14,16].

Testing inside animal tissue can be performed by implanting antenna inside tissue samples from donor animals, or by surgically implanting the antenna inside live model animals. In the first case, electrical properties of the test tissue can be measured using a dielectric probe kit and a network analyzer. The use of animal tissue samples provides an easy approach to mimic the frequency dependency characteristics of the electrical properties of tissues. This can prove highly advantageous when carrying out measurements for multi-band implantable antennas. In the literature, an implantable patch antenna with dual resonances at 380 and 440 MHz was tested inside test tissue obtained by grinding the front leg of a pig [18]. The electrical properties of the adapted pork were found to be between those of human skin and muscle in the ISM band. A dual-band skin-implantable patch antenna operating in the MICS and 2450 MHz ISM bands was also tested in real animal skin [21].

Recipes proposed mainly included ultra pure water, sugar, and salt. An increase in sugar concentration has been found to significantly decrease  $\epsilon_r$ , while slightly increase  $\sigma$ . An increase in salt concentration decreases  $\epsilon_r$  and significantly increases  $\sigma$  [11]. Adding gelatin or dry agarose to solidify the liquids and form multilayer gel phantoms was also examined [21]. The proposed antenna is fabricated with biocompatible alumina ceramic

**Fig. 13.** Measurement setup in pork tissue and phantom model.

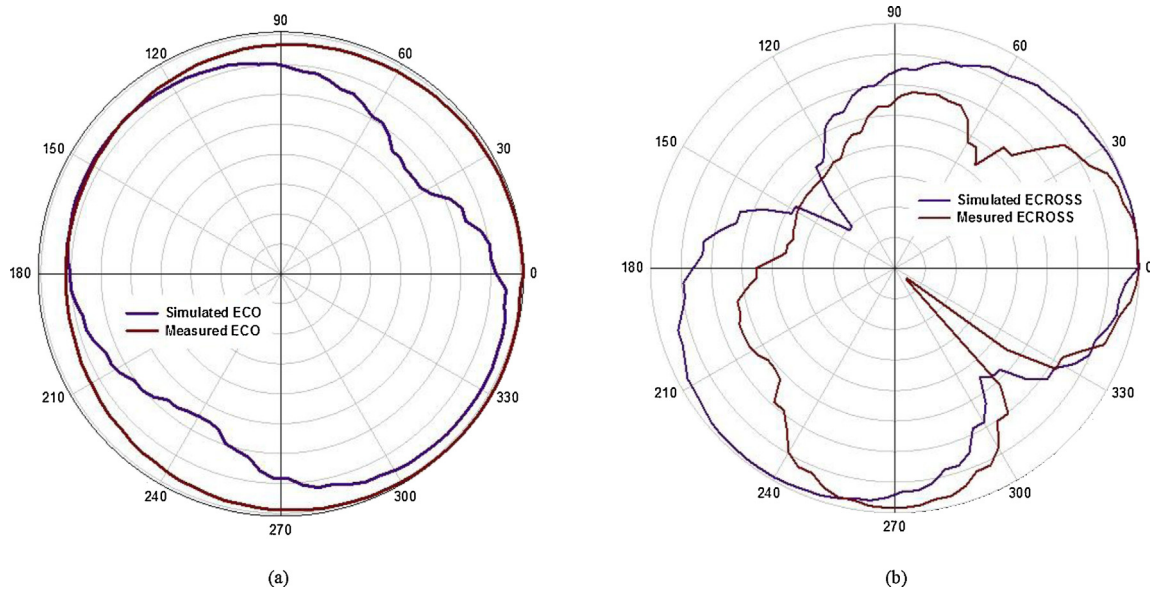


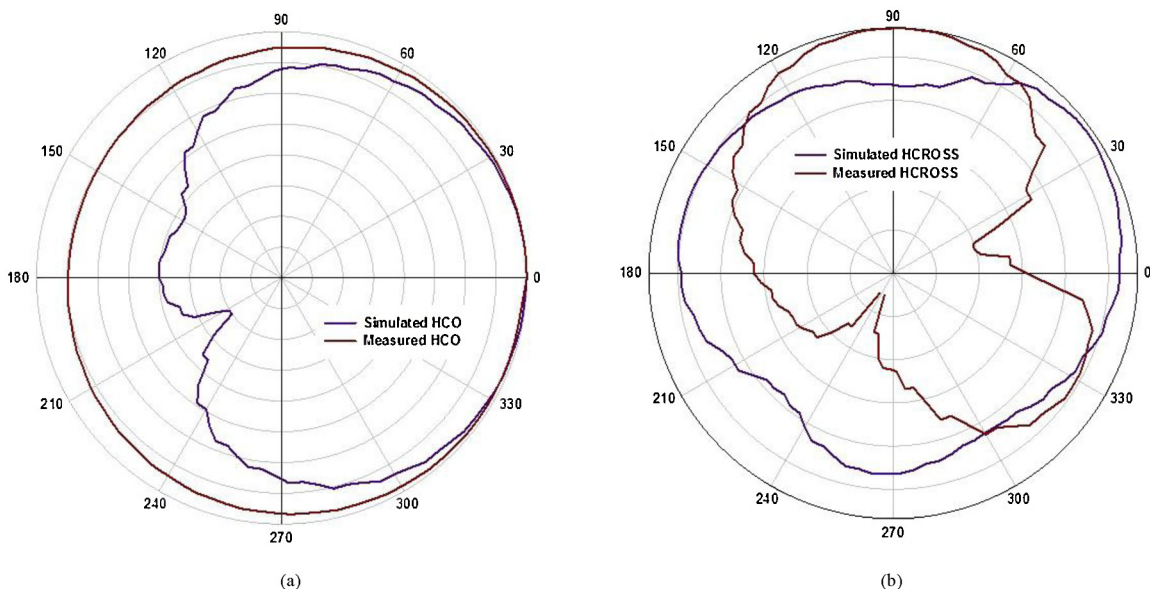
**Fig. 14.** Measured radiation pattern for E-field at 2.45 GHz. (a) Co polarization and (b) cross polarization.

substrate ( $\epsilon_r = 9.8$ ,  $h = 0.5$  mm) as shown in Fig. 11. For measuring the antenna parameters like return loss, Radiation Patterns are calculated with help of Vector Network Analyzer and anechoic chamber as shown in Figs. 12 and 13.

The radiation characteristics of the antenna inside the liquid simulating muscle fat skin tissue are determined in terms of radiation patterns and gain. To simulate, the antenna is directed toward the surface of the gel (muscle, fat and skin) and along the z-direction the distance to the surface of the gel is set to 12 mm in the xy-plane, the antenna is placed in the center of the surface of the human model phantom. The computed radiation patterns in the E-plane and H-plane are shown in Figs. 14 and 15, respectively. The patterns are computed at 2.45 GHz, at a reference distance of 1 m and using an input power of 1 W. The maximum gain is equal to  $-6$  dBi for  $\theta = 0$  and  $\varphi = 0$  and the radiation efficiency is 0.14%. The radiation efficiency is very low because the antenna is not in free space, but embedded into human tissue, simulated as a very lossy tissue

medium. Discrepancy between simulated and measured radiation pattern shows that there are some differences between the two patterns especially at the lower half of the pattern where the present of the side lobes in measured radiation pattern is significant. This variation can be explained in view of the SMA connector which was connected to the antenna which may act as a significant scatterer. For H-plane, both patterns are quite similar with the only difference is on the plane due to the existence of radiation from the surrounding environment.

Finally, an implantable antenna was tested inside a minced front leg of a pig. The electrical properties of the minced pork were measured, and return loss characteristics of pork tissue, human phantom liquid and simulated results are plotted in Fig. 16. It can be found to correspond to those of human skin and muscle between 300 MHz and 3 GHz. Comparison results of simulated and measured values are reported in the Table 3. In vivo investigations are also vital in order to investigate the

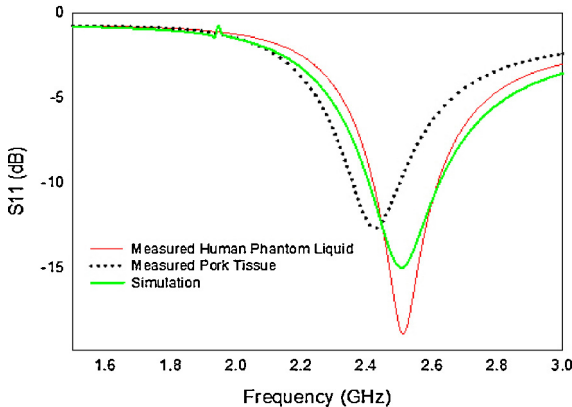


**Fig. 15.** Measured radiation pattern for H-field at 2.45 GHz. (a) Co polarization and (b) cross polarization.

**Table 3**

Comparison results of simulated and measured results.

S. No.	Parameters	Frequency (GHz)	Simulated results	Measured results
1	Return loss	2.45	-23 dB	-26 dB
2	VSWR	2.45	1.0	1.1
3	Impedance matching	2.45	23%	24.62%
4	Antenna gain	2.45	-6 dBi	-6.5 dBi
5	Antenna efficiency	2.45	0.25%	0.2%

**Fig. 16.** Return loss comparison vs frequency.

effects of live tissue on the performance of implantable antennas, while providing valuable feedback for antenna design and analysis.

#### 4. Conclusion

In this paper, a novel implantable CPW fed crossed bowtie antenna for biomedical applications is presented with a compact size of ( $26\text{ mm} \times 22\text{ mm} \times 0.65\text{ mm}$ ) and solutions suggested regarding the design, numerical simulations, and experimental investigations of implantable CPW fed crossed bowtie antenna for biomedical telemetry. The design of implantable antennas mainly emphasizes miniaturization and biocompatibility. Conserving energy to extend the life span of the implantable medical device is also significant. ISM band antennas are being designed for these purposes that “wake up” the implantable medical device only when there is a need for information exchange.

The numerical simulations of implantable CPW fed bowtie antennas are based on the transmission line model. Several methods have been proposed for implantable antenna design, all of which need to take into the swarm body. A homogenous model is plenty for antenna design, a more sensible model is needed to refine the antenna design and provide perfect results. Due to better dielectric constant of the alumina ceramic substrates, implantable antenna exhibit miniaturization, lower return loss, good VSWR, better impedance matching and high gain compared to over the other implanted antennas (Table 4). Therefore, the

proposed antenna is the suitable candidate for ISM band frequency of 2.45 GHz in the field of Biomedical Engineering.

#### References

- [1] Scarpello ML, Kurup D, Rogier H, Vande Ginste D, Axisa F, Vanfleteren J, et al. Design of an implantable slot dipole conformal flexible antenna for biomedical applications. *IEEE Trans Antennas Propag* 2011;59(October (10)):3556–64.
- [2] Huang FJ, Lee CM, Chang CL, Chen LK, Yo TC, Luo CH. Rectenna application of miniaturized implantable antenna design for triple-band biotelemetry communication. *IEEE Trans Antennas Propag* 2011;AP-59(July (7)):2646–53.
- [3] Hadarig RC, María Elena de Cos Gomez F, Las-Heras F. Novel Bowtie–AMC combination for 5.8-GHz RFID tags usable with metallic objects. *IEEE Antennas Wireless Propag Lett* 2010;9:1217–20.
- [4] Karacolak T, Hood AZ, Topsakal E. Design of a dual-band implantable antenna and development of skin mimicking gels for continuous glucose monitoring. *IEEE Trans Microw Theory Techn* 2008;56(April (4)):1001–8.
- [5] Huang L, Ashouei M, Yazicioglu F. Ultra-low power sensor design for wireless body area networks: challenges, potential solutions, and applications. *JDCTA* 2009;3(September (3)).
- [6] Kim J, Rahmat-Samii Y. Implanted antennas inside a human body: simulations, designs, and characterizations. *IEEE Trans Microw Theory Techn* 2004;52(August (8)):1934–43.
- [7] Warty RM, Tofghi R, Kawoos U, Rosen A. Characterization of implantable antennas for intracranial pressure monitoring: reflection by and transmission through a scalp phantom. *IEEE Trans Microw Theory Techn* 2008;56(October (10)):2366–76.
- [8] Lee CM, Yo TC, Huang FJ, Luo CH. Band width enhancement of planar inverted-F antenna for implantable biotelemetry. *Microw Optic Technol Lett* 2009;51(March (3)):749–52.
- [9] Karacolak T, Cooper R, Topsakal E. Electrical properties of rat skin and design of implantable antennas for medical wireless telemetry. *IEEE Trans Antennas Propag* 2009;57(September (9)):2806–12.
- [10] Sánchez-Fernández CJ, Quevedo-Teruel O, Requena-Carrión J, Inclán-Sánchez L, Rajo-Iglesias E. Dual-band microstrip patch antenna based on short-circuited ring and spiral resonators for implantable medical devices. *IEEE Trans Microw Antennas Propag* 2010;4(August (8)):1048–55.
- [11] Skrivenik AK, Merli F. Design strategies for implantable antennas. In: Proceedings of the antennas and propagation conference. 2011.
- [12] Abadía J, Merli F, Zurcher JF, Mosig JR, Skrivenik AK. 3D Spiral small antenna design and realization for biomedical telemetry in the MICS band. *Radioengineering* 2009;18(December (4)):359–67.
- [13] Lee CM, Yo TC, Luo CH. Compact broadband stacked implantable antenna for biotelemetry with medical devices. In: Proceedings of the IEEE annual conference on wireless microwave technology, clear water. 2006.
- [14] Karacolak T, Cooper R, Butler J, Fisher S, Topsakal E. In vivo verification of implantable antennas using rats as model animals. *IEEE Antennas Wireless Propag Lett* 2010;9:334–7.
- [15] Kiourti A, Nikita KS. Miniature scalp-implantable antennas for telemetry in the MICS and ISM bands: design, safety considerations and link budget analysis. *IEEE Trans Antennas Propag* 2012;60(8):3568–75. <http://dx.doi.org/10.1109/TAP.2012.2201078>.
- [16] Kawoos Ü, Tofghi MR, Warty RF, Kralick A, Rosen A. In-vitro and in-vivo trans-scalp evaluation of an intracranial pressure implant at 2.4 GHz. *IEEE Trans Microw Theory Techn* 2008;56(October (10)):2356–65.
- [17] Huang W, Kishk AA. Embedded spiral microstrip implantable antenna. *Int J Antennas Propag* 2011:1–6.
- [18] Italian National Research Council, Institute for Applied Physics, Dielectric properties of body tissues, <http://niremp.ifac.cnr.it>
- [19] Merli F, Skrivenik AK. Design and measurement considerations for implantable antennas for telemetry applications. In: Proceedings of the 4th European conference on antennas and propagation (EuCAP 2010). 2010.
- [20] Sani A, Rajab M, Foster R, Hao Y. Antennas and propagation of implanted RFIDs for pervasive healthcare applications. *Proc IEEE* 2010;98(September (9)):1648–55.

**Table 4**

Comparison results of other implanted antennas.

References	Dimensions ( $\text{mm}^3$ )	Gain (dBi)	10 dB Bandwidth (MHz)
[10]	1524.0	-16	12
[4]	1265.6	-25	142
[8]	790.9	-27	120
[13]	385.8	-26	50
This paper	371.8	-6	190

- [21] IEEE Standard for safety levels with respect to human exposure to radio frequency electromagnetic fields, 3 kHz to 300 GHz. IEEE Standard C95.1-1999 2012.
- [22] Simons RN. Coplanar waveguide circuits, components and systems. John Wiley & Sons, Inc.; 2001.



**S. Ashok Kumar** received B.E. degree in Electronics and Communication Engineering from Anna University, Chennai, India, in 2006 and M.E. degree in Applied Electronics from Thanthai Periyar Government Institute of Technology, Anna University, Chennai, India, in 2009. He has two years of teaching experience in Adhiparasakthi Engineering College, Melmaruvathur. He is currently working toward the Ph.D at Department of Electronics Engineering, School of Engineering and Technology, Pondicherry University (Central University), Pondicherry, India. He has authored for one book chapter and 16 journal and conference papers. His current research interest includes antenna theory, biomedical telemetry and implantable antennas.



**T. Shanmuganantham** received B.E. degree in Electronics and Communication Engineering from University of Madras in the year 1996, M.E. degree in Communication Systems from Madurai Kamaraj University in the year 2000 and Ph.D. (Gold Medal) in the area of Antennas from National Institute of Technology, Tiruchirappalli, India in the year 2010 under the guidance of Dr. S. Raghavan. He has 15 years of teaching experience in various reputed Engineering colleges such as SSN College of Engineering, National Institute of Technology and Science. Presently he is working as Assistant Professor in Department of Electronics Engineering, School of Engineering & Technology, Pondicherry University, Pondicherry. His research interest includes Antennas, Microwave/Millimeter-Wave Circuits and Devices, Microwave Integrated Circuits, EMI/EMC, Computational Electromagnetics, MEMS/NEMS, Metamaterials. He has published 75 research papers in various national and International level Journals and Conferences. He has completed one sponsored project and 2 projects are in the pipeline. He is a coordinator for MEMS Design Center, NPMASS. His biography was included in Marquis Who is Who in the World, USA in the year 2010. He is a member in IEEE, Life Member in IETE, Institution of Engineers, CSI, Society of EMC, ISSS, OSI, ISI, ILA and ISTE.